UNIVERSITÀ DEGLI STUDI DI PADOVA

Dipartimento di Ingegneria Industriale

Corso di Laurea Magistrale in Energy Engineering

Dynamic simulation of an integrated thermal electricity storage system using Aspen Plus Dynamics

Relatore: Prof.ssa Anna Stoppato
Correlatore: Ing. Simone Peccolo

Laureando:
Alessandro Lecchi
Matricola 2085756

Anno Accademico 2023/2024

Abstract

The increment of greenhouse gas emissions from human activities have forced the world authorities to ratify stringent measures devoted to the reduction of primary energy consumption and to the spread of Renewable Energy Sources (RES). However, the widespread adoption of variable and intermittent RES highlights the necessity for large-scale energy storage, but available technologies, like Pumped Hydro, Compressed Air Energy Storage or Flow Batteries, suffer from geographical constraints, require fossil fuel streams or are characterized by low cycle life. In this context, Thermal Energy Storage Systems are poised to play a fundamental role due to their long cycle life, lack of geographical limitations, absence of fossil fuel requirements and compatibility with integration into conventional fossil-fuelled power plants.

Based on this evidence, in the present study, the dynamic behaviour of an Integrated Thermal Electricity Storage System using Aspen Plus has been investigated. Aspen Plus is a pivotal tool for modelling both steady-state and dynamic systems, enabling the connection of components from its software library through streams. In instances where a specific component is not available in the library, Aspen Modeler can be utilized to model it, and subsequently, it can be integrated into Aspen Plus. This is exemplified in this study, where a packed bed is modelled using Aspen Modeler and incorporated into the overall system analysis.

Riassunto in lingua italiana

L'aumento delle emissioni di gas serra provenienti dalle attività umane ha spinto le autorità mondiali ad adottare misure severe per ridurre il consumo di energia primaria e per diffondere le Fonti Energetiche Rinnovabili (FER). Tuttavia, l'ampio sviluppo di FER variabili e intermittenti evidenzia la necessità di grandi sistemi di stoccaggio dell'energia, ma le tecnologie disponibili, come il pompaggio idroelettrico, lo stoccaggio di energia ad aria compressa o le batterie a flusso, presentano limitazioni geografiche, richiedono l'utilizzo di combustibili fossili o hanno una vita utile limitata. In questo contesto, i sistemi di stoccaggio dell'energia termica possono svolgere un ruolo chiave grazie alla loro lunga durata, alla mancanza di limitazioni geografiche, all'assenza di combustibili fossili e alla compatibilità con l'integrazione nelle centrali elettriche convenzionali a combustibili fossili.
Pertanto in questo lavoro di tesi, dopo un'iniziale panoramica sulle principali tecnologie di stoccaggio dell'energia (elettrochimico, meccanico, elettromagnetico, termodinamico, chimico e ibrido), è fornita una dettagliata descrizione dei promettenti Pumped Thermal Electricity Storage (PTES) e Integrated Thermal Electricity Storage System (IT-ESS), entrambi sistemi di accumulo il cui principio di funzionamento è immagazzinare elettricità sotto forma di energia termica.
L'obiettivo principale della tesi è la modellazione di un sistema IT-ESS in ambiente Aspen Plus, strumento utile per modellare sistemi sia in condizioni stazionarie che dinamiche e che permette di collegare componenti dalla sua libreria per formare sistemi anche complessi; tuttavia, la mancanza nella libreria del software di un componente in grado di descrivere il comportamento del serbatoio rende necessario l'utilizzo di Aspen Custom Modeler, sottosistema di Aspen Plus che consente di modellare un componente inserendo le equazioni che ne descrivono il comportamento in un linguaggio specifico e successivamente ne permette l'integrazione in Aspen Plus. Dunque, parte della tesi è dedicata alla costruzione del prototipo di un accumulo termico basato sulle equazioni del modello di Benato.
In seguito, l'integrazione dell'accumulo con i restanti componenti del sistema IT-ESS permette di condurre simulazioni di processi di carica e scarica con differenti parametri operativi. Dopo aver fatto alcune simulazioni con determinate variabili indipendenti, è stata fatta un'analisi di sensibilità per valutare l'impatto della variazione di alcuni parametri sul sistema complessivo.
Infine, sono stati proposti possibili sviluppi futuri, con accenni all'aggiunta di sistemi di controllo e all'incorporazione delle curve caratteristiche di compressore e turbina, per migliorare la precisione del modello rispetto al comportamento reale dell'impianto.

Contents

Chapter 1

Introduction

With the advancement of technology, humanity has transitioned from an industrial civilization to an ecological one, moving from wasteful and extensive consumption to more economical and efficient practices, and from high carbon emissions to low carbon production. The current global energy paradigm, dominated by fossil fuels, is gradually shifting towards a diversified energy structure, eventually favoring non-fossil energy sources. In this context, the development of distributed photovoltaic (PV) generation systems has seen remarkable growth over the past two decades. These systems are characterized by their adaptability to local conditions, cleanliness, efficiency, decentralized layout and local consumption.

The International Energy Agency projects that solar power will become a significant mainstream energy source by 2050, contributing approximately 11% to global electricity generation. Most of these PV systems have been and will continue to be installed in distribution networks, leading to unprecedented levels of PV penetration, exceeding 50% in many distribution networks worldwide. However, such high penetration poses significant technical challenges including voltage regulation, harmonics, grid protection, and more [1]. An emblematic example is represented by the Italian wind and photovoltaic (PV) sectors (data available on [2]). In 2006, the PV plants were 14 with an installed power and an annual gross electricity production equal to 7.17 MW and 2.3 GWh, respectively. In 2007, the PV plants have become 7647 with an installed power of 86.80 MW and an annual gross electricity production equal to 39.10 GWh. An increment of 1109.3% of the installed power in one year. After 10 years (2016), the installed PV plants were 732053 while their power and annual gross electricity production were 19283.17 MW and 22104.3 GWh, respectively. In 2022, the total number of plants was around 1 million 200 thousand, with a strong increase in 2023.

A similar trend is observed in the wind power sector. In 2006, there were 169 installed wind turbines, which increased to 3598 by 2016 and to more than 7000 by 2022. The installed capacity and annual electricity production also rose signifi-

cantly over the same period. Wind, solar, hydro, etc. are environmentally friendly energy sources which guarantee to produce electricity in eco-friendly ways but, unlike the hydroelectric power, wind and solar production suffer of high variability, unpredictability and uncontrollability, characteristics which cause large fluctuations in their daily, monthly or even annually power production. In fact, as in the Italian case, the large number of plants fed by Variable Renewable Energy Sources (VRES) added to the traditional electric grid introduces management and control issues because, with a high number of users and producers, the demand and the plants production become difficult to forecast. Thus, there can be areas characterised by over-capacity and areas with under-capacity. Unbalances between production and demand are difficult to predict and manage and can cause local o even global blackouts. Note that the above-mentioned issues will grow with the increment of VRES plants because, as remarked in [3], the grid is able to absorb fluctuations only if the VRES power is up to 10% of the system installed capacity.
Addressing these challenges requires the development and installation of large-scale electric energy storage systems to manage the disparity between supply and demand. The International Energy Agency estimates a need for significant capacity expansion worldwide by 2040 to meet rising energy demands. Additionally, substantial electric energy storage capacity must be built in regions like the US, Europe, China, and India to accommodate the integration of intermittent and non-flexible power sources into the grid [4],[5].
Figure 1.1 illustrates the trend from 2014 to 2024, depicting the anticipated overlap and eventual surpassing of electricity generation from renewable sources compared to coal in the coming years.

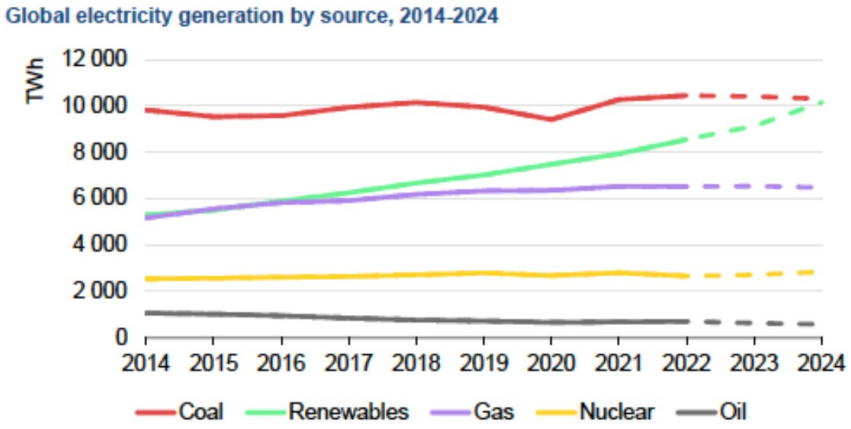

Figure 1.1: Global electricity generation by source, 2014-2024 [4].

In this scenario, the available large-scale Electricity Storage Technologies (ESTs), like Pumped Hydro Storage (PHS) or Compressed Air Energy Storage (CAES), can play a fundamental role, but due to their need of suitable geographical sites,

these energy storages (ESs) can be built only in countries with favourable morphology. Therefore, alternative ESTs need to be explored.
Pumped Thermal Electricity Storage (PTES) or Pumped Heat Energy Storage (PHES) can become a valuable technology able to store large quantity of energy in a cheap way especially if they use Sensible Heat Thermal Energy Storage (SH-TES). In addition, PTES units can contribute to the challenging process of integrating ESs into fossil-fuelled power plants (FFPPs) or in their re-powering. In the first case, PTES can help into the reduction of FFPPs fast ramp rates, possible low load levels, cycling operations and overnight shut-downs while, in the second case, the components of an underutilised fossil-fuelled power plant can be partially reused to build the PTES unit [6]. Therefore, it is clear that the need of energy storage devices is increasing with the increase of renewable energy penetration and in the following years a sharp increase in global cumulative energy storage installations is expected, as clearly shown in Figure 1.2.

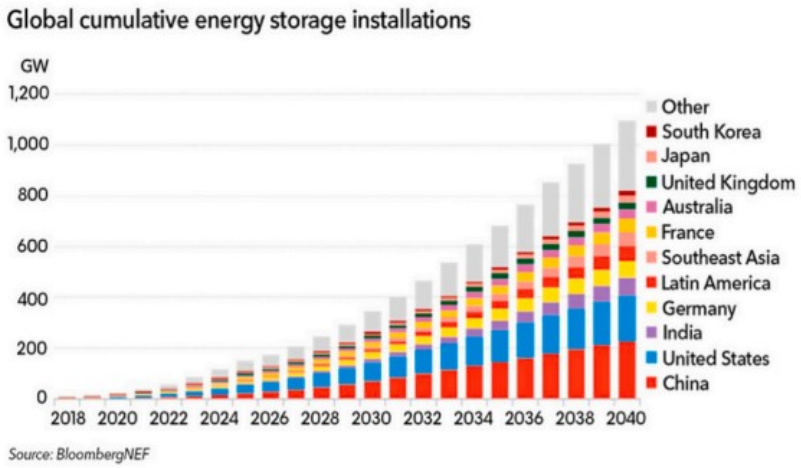

Figure 1.2: Prediction of the instalments of energy storages until 2040 [7].

In this optic, there is an urgent need to investigate and develop new solutions and strategies in the energy storage sector; in the next chapter all the existing technologies are quickly reviewed, highlighting positive and negative aspects of each, then the attention will shift towards the Integrated Thermal Electricity Storage Systems.

Chapter 2

Energy storage technologies overview

To start, the concept of energy storage is introduced.
According to Benato and Stoppato [6], an energy storage is a device or a system in which the energy can be stored in a certain form. In a second moment, this energy can be extracted to perform some useful operations. The process of storing can be subdivided into three main phases: charging, storing and discharging. During the first phase, the energy enters the storage device. Then, during the second phase, the energy remains inside the storage system and during the discharging phase it is released.
It is well known that there are several forms of energy, but they can be mainly grouped in two categories: primary and secondary form of energy. The first category includes all the energy forms which are not subjected to any kind of conversion or transformation process. Coal, natural gas, crude oil, wind, solar, tidal, geothermal, falling water, etc. are primary energy forms while electricity, heat, hydrogen, gasoline, diesel, etc. are secondary forms of energy because they are a product of a conversion or transformation process from other energy forms. Based on this classification, also energy storage can be classified as primary and secondary energy storage. Coal, natural gas, crude oil, and biomass are primary forms of energy that are easy to store in their natural state.
Wind, solar, tidal and wave are also primary energy forms, but they are storable only after a transformation into a secondary energy forms like electricity, heat or work. Storing secondary energy forms is an easy process, while stocking work, heat and electricity is a really challenging process but can contribute to spread VRES and help to diminish fossil fuel consumption, which in turns results in a cut of CO_2 and greenhouse gases emissions. Gasoline, diesel, hydrogen, methane, biofuels, etc. are easily storable in tanks, containers or pressurized vessels while heat and electricity need to be stocked using different kind of materials usually called "energy carriers". In a nutshell, during the charge, the energy source is stored by means of an energy carrier while, during delivery, the stocked energy is returned to supply the energy demand.

In literature there are several ways to classify energy storage technologies; in this work, the classification follows Amir and Deshmukh [8].
For ESSs, a variety of technologies are deployed. The numerous types of ESTs are depicted in Figure 2.1.

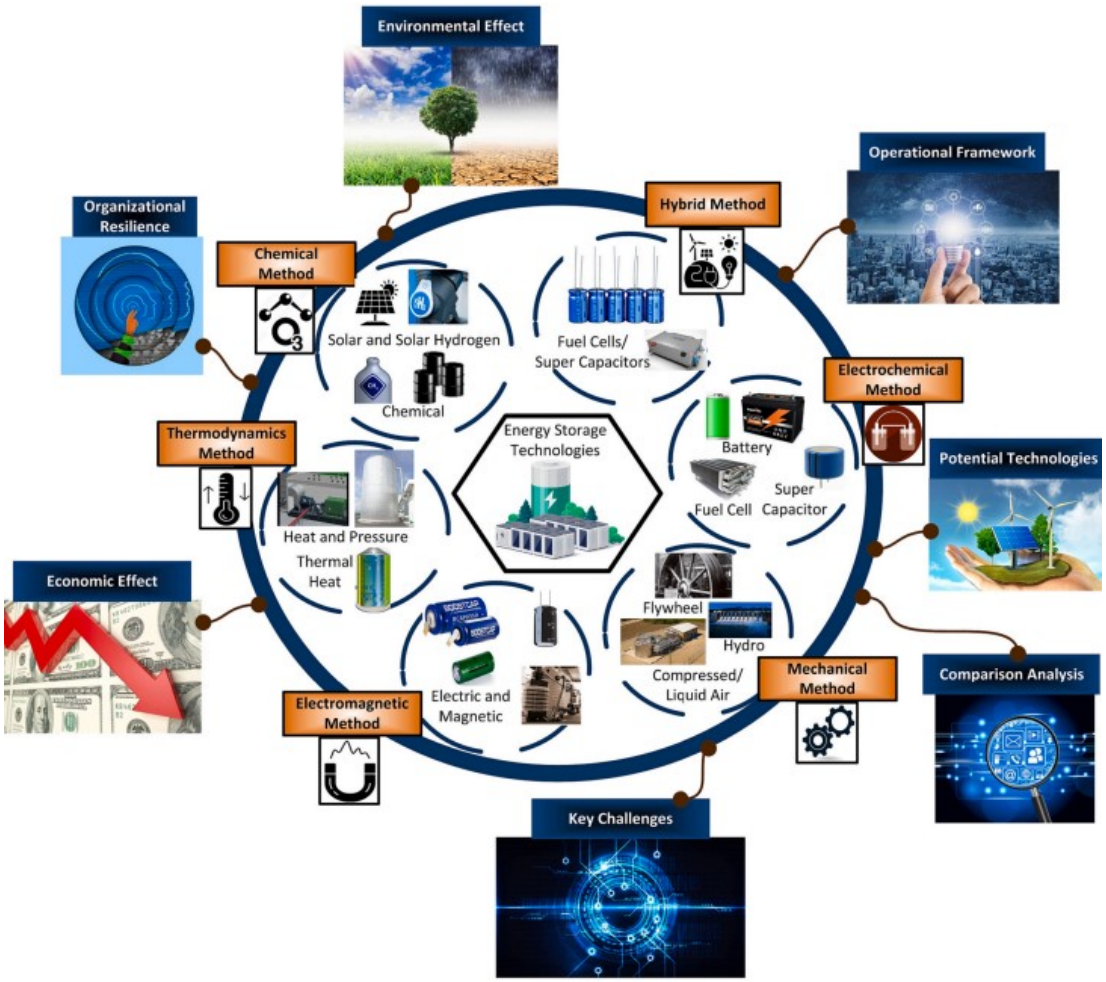

Figure 2.1: EST interaction [8]

Out of these categories, mechanical ES, solar fuel cell, hydroelectric pumping storage, chemical (hydrogen ES), electrochemical (supercapacitor ES, battery ES), superconducting magnetic energy storage (SMES), and TES are all classified as electrical ES methods. ST includes a range of devices that can be divided into six wider categories, such as:

- electrochemical ST;
- mechanical ST;
- electromagnetic ST;
- thermodynamic ST;

- chemical ST;
- hybrid-based technologies ST.

Note the enhanced EST are adept at dispatching energy (msec or sec), backup storage (few mins to several hrs), appropriate duration (shorter or longer), response time, rating of EST (kWh and MWh). This allows selecting the suitable technology based on desired applications.

2.1 Electrochemical method

When the ES is processed in supercapacitors, it is also known as electrochemical storage, which could be in the form of electrochemical capacitors, ultra-capacitors, or electric double-layer capacitors [9]. Here, faster ESSs were required in various applications to replace Li-ion batteries that suffered from slow charge/ discharge and have a short lifetime. Compared to traditional capacitors, the supercapacitor has a substantially higher capacitance, energy density and compactness. The two series capacitors of the electric double layer created between each electrode and the electrolyte ions store energy in supercapacitors. They have a high energy density and can respond in tens to hundreds of milliseconds to any change in power demand. The most pressing task for the supercapacitor is to lower its cost and enhance its energy density to $<$10 Wh/kg, bringing it closer to batteries. Increasing the capacitance and/or cell voltage is one approach to accomplish this. Supercapacitors have a practically infinite number of charge and discharge cycles, but their energy throughput in fast cyclic operation is restricted. Supercapacitors have a 95 % efficiency and a 5 % self-discharge rate each day, implying that the stored energy must be used immediately. Either directly or indirectly, electrochemical ES converts stored energy into electricity. Both flow and solid-state batteries are tiny and portable in this division.
Using batteries, chemical energy is converted to electrical energy. As technology advances and costs decrease, grid-scale battery storage solutions are becoming more popular. The ES at moss landing facility in California, the first 300 MW Li-ion battery with 4500 stacked battery racks started operationally in January 2021 [10]. Australia, Germany, Japan, the United Kingdom, Lithuania, and Chile are all considering installing large-scale battery energy systems.
The secondary or rechargeable battery is considered the oldest type of electrical ES device. It stores electrical energy as chemical energy through electrochemical reactions, and can release the energy in the form of electrical energy as needed. Batteries are manufactured in various sizes and can store anywhere from $<$100 W to several MWs of energy. Their efficiency in energy storage and release, known as roundtrip ES efficiency, is between 60 and 80 %, and this depends

on the operational cycle and the type of electrochemistry used. Batteries are the most commonly used type of ES device for power system applications due to their widespread availability and reliability. In addition to being used for electric grids, batteries are used in many other sectors such as hybrid electric vehicles (HEV), marine and submarine missions, aerospace operations, portable electronic systems and wireless network systems. There are various types of batteries that are suitable for different applications. Deep cycle batteries are the most commonly used type for power system applications, and they have an efficiency range of 70–80 % [8]. Then, Amir and Deshmukh [8] presented several different kind of batteries; in the present work, the analysis is limited to Lithium-Ion (Li+) batteries, being those that are used in electric vehicles; hence, hopefully, in the next years, their production will be more efficient as fossil-fueled cars are abandoned. Li-ion batteries are made of two low density lithium components and have a large standard electrical potential making them the main electronic handler. These are low weight, high voltage without a memory, low self-loads and internet-of-things (IoT). Li-ion batteries are used for the mobile and various applications of electric vehicles, but it is too expensive for large-scale grid storage. However, Li-ion batteries have an extensive impact on the depletion of metals and can therefore cause significant environmental, social and health impacts on the toxicity and site of lithium mining in the natural environment. A Li-ion battery is made up of various cells that interlink to another call. Every cell comprises three major parts such as a cathode, an anode and a liquid-based electrolyte, as depicted in Figure 2.2. The toxicity of Li-ion batteries is, to be sure, lower than that of many other batteries [8].

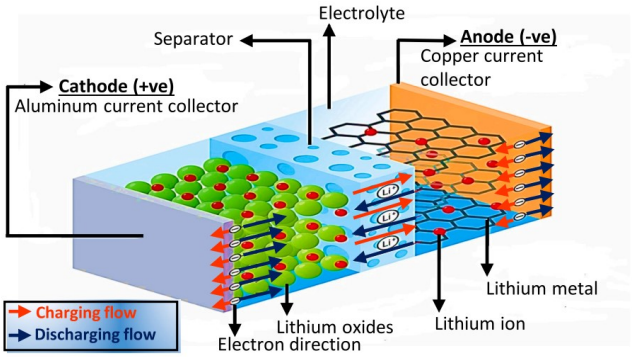

Figure 2.2: Diagram of the Li-ion battery with charging and discharging flow, [8].

In addition to battery and supercapacitor, a third kind of electrochemical storage is constituted by the flow cell or redox flow cell (after reduction-oxidation), which is a type of electrochemical cell where electricity is generated by the potential difference between the tanks in these batteries. Both tanks' solutions become the same, containing both positive and negative ions. The most frequent ma-

terials utilized in these batteries are vanadium polyamide, vanadium hydrogen bromine, bromine polysulfide, and iron-chromium. A sketch of the operation of such a battery is reported in Figure 2.3. In hybrid-based flow batteries, a single

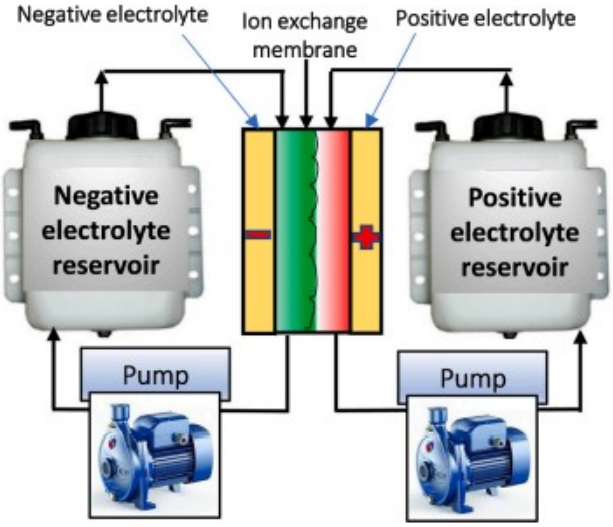

Figure 2.3: Operational framework of a Redox flow battery, [8].

or high number of electroactive components are employed as a solid layer. As a result, two liquid electrolytes containing metal ions dissolved in the fluid electrolyte do not change phase. An ion-selective membrane is used to separate the negative and positive redox ions. These batteries have high efficiency, long cycle life, flexible design, and high ES capacity, whereas their density is low compared to others.

Finally, energy can also be stored in chemical form, such as hydrogen. The potential versatility of this low-density gas for storing and transmitting energy has led to extensive research over the past few decades, garnering increasing attention in the energy sector. Hydrogen's adaptability for various end-uses includes serving as a fuel for electricity and/or heat production in fuel cells or combustion engines, as well as powering transportation devices. Additionally, hydrogen serves as a chemical commodity, further expanding its potential applications [11].

2.2 Mechanical method

Mechanical energy may be stored as the kinetic energy of linear or rotational motion, as the potential energy in an elevated object, as the compression or strain energy of an elastic material, or as the compression energy in a gas. It is difficult to store large quantities of energy in linear motion because one would have to chase after the storage medium continually. However, it is quite simple to store rotational kinetic energy.

Compressed air energy storage (CAES) and pumped hydro energy storage (PHES) are the most modern techniques.
Pumped Hydro Storage or Pumped Hydroelectric Energy Storage is the most mature, commercially available and widely adopted large-scale energy storage technology since the 1890s. The PHS technology uses gravity to store the electrical energy and a typical plant layout consists of an upper and a lower reservoirs, a waterfall, pipes, a pump, a turbine, an electric motor and an electric generator. The pump and the turbine can be separated machines or the same device supplies both the functions. In the second case, the turbomachine is called reversible pump-turbine. Also the electric machine can be separated devices (a motor which moves the pump and a generator connected to the turbine) or a unique electrical machine (a motor/generator). A sketch of the PHS system is depicted in Fig. 2.4. The fundamental concept of Pumped Hydro Storage (PHS) is quite straightforward. During off-peak periods, electricity is drawn from the grid and used to power an electric motor, which in turn drives a pump. This pump moves water from a lower reservoir to an upper reservoir, effectively storing energy. Then, during periods of high demand, the stored water is released from the upper reservoir to the lower reservoir through a turbine. The turbine is connected to an electric generator, converting the mechanical energy from the flowing water into electrical energy, which is then fed back into the electric grid.

PHS technology currently accounts for approximately 99% of large-scale energy storage installations worldwide [6].

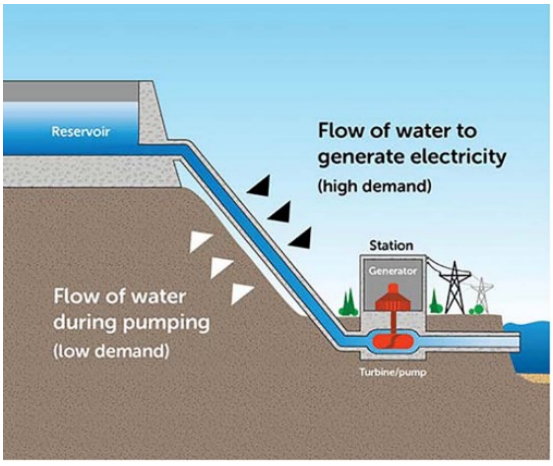

Figure 2.4: Sketch of a Pumped Hydro Storage Unit, [12].

Compressed Air Energy Storage (CAES) stands as the second commercially available large-scale energy storage technology. During periods of low power demand, surplus generation capacity is utilized to compress air, storing it either in underground caverns (such as hard rock caverns, salt caverns, depleted gas fields, aquifers, etc.) or in aboveground man-made tanks, pipes, containers, or

vessels. Subsequently, during high peak demand hours, the pressurized air is extracted from storage, heated (often using natural gas) and expanded in an air turbine. With the air turbine mechanically linked to an electric generator, the potential energy of the pressurized air is converted back into electricity. This type of CAES facility is termed Diabatic CAES (DCAES) because, during the compression phase, the heat generated is discarded.

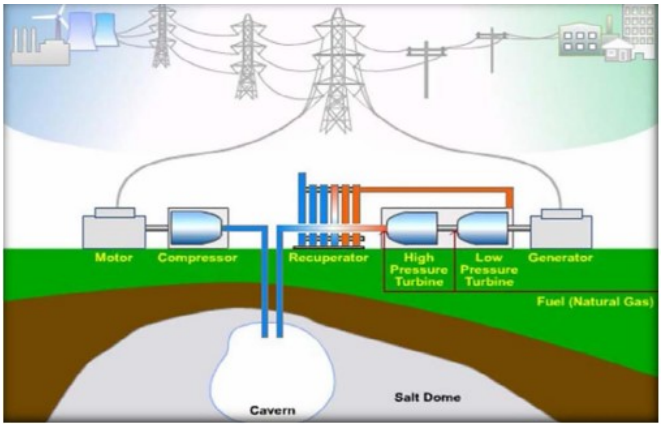

Figure 2.5: Sketch of a Compressed Air Energy Storage Unit, [13].

Over the years, researchers have explored and developed various plant configurations with the goal of reducing fuel consumption, recovering heat generated during the compression process and addressing geographical constraints. Adiabatic CAES (ACAES), Isothermal CAES (I-CAES), and Underwater CAES (UW-CAES) represent upgraded versions of Diabatic CAES.

Despite these advancements, both CAES and PHS share a common drawback: they necessitate specific site morphologies for installation. However, to date, CAES remains the sole technology capable of competing with PHS for large-scale energy storage applications, despite its reliance on fossil fuel streams.

At this juncture, it is worth considering the following: comparisons among the available large-scale energy storage technologies mentioned above indicate that Pumped Hydro Storage (PHS) will likely continue to dominate in the near future. However, it is anticipated that Compressed Air Energy Storage (CAES) and Flow batteries will experience rapid development. Despite this projection, there is an urgent need to develop new large-scale Energy Storage Technologies (ESTs) that do not face geographical limitations (as with PHS and CAES), low cycle life (as seen in flow batteries), high capital costs and reliance on fossil fuels [6].

Liquid Air Energy Storage (LAES) is another emerging large-scale storage technology that involves storing electrical energy in the form of liquefied air. Similar to CAES technology, the initial step of the charging phase involves compressing air. Subsequently, the pressurized air is liquefied and stored in thermally isolated man-made vessels, tanks, or containers. During discharge, the liquid air

is heated using a heat exchanger, which increases also the pressure. The high-pressure air is then utilized to drive an expansion machine mechanically connected to an electric generator.
The primary advantages of LAES include its high energy density (50 Wh/l or 97–210 Wh/kg) and the significantly smaller volume occupied by liquid air compared to its gaseous form (1/700). This characteristic leads to a drastic reduction in the volume of storage vessels. In fact, an LAES plant can be up to 12 times smaller than a CAES plant and up to 140 times smaller than a PHS plant [6].

Gravity Energy Storage (GES) systems have been studied as a solution to address the primary drawbacks of Pumped Hydro Storage (PHS), namely the requirement for a sufficient water flow and specific geographical morphologies at installation sites. The GES system operates as a closed-loop configuration, consisting of a deep storage shaft, a return pipe, a large piston, and a reversible pump-turbine, with water serving as the working fluid. The large piston, equipped with substantial sliding seals to prevent leakage, is suspended within the deep storage shaft.
During periods of low demand, off-peak electricity is utilized to pump water from the deep storage shaft to the return pipe, causing the large piston to ascend from the bottom to the top of the shaft. Conversely, during peak demand periods, the large piston descends from the top to the bottom of the shaft, propelling the water through the return pipe. This water then powers a hydraulic turbine, generating electrical energy. Despite the absence of Gravity Power Modules (GPM) installations, this storage technology is expected to achieve a round-trip efficiency exceeding 80%.
In contrast to PHS, the GES system operates as a closed-loop, obviating the need for a continuous water flow, and it does not necessitate natural waterfalls as the deep storage shaft and return pipe are man-made channels. However, like PHS and Compressed Air Energy Storage (CAES), GES installations require sites with stable morphologies. Additionally, due to the system's complexity, investment costs are comparable to those of PHS (ranging from $600 to $2000 per kilowatt) and CAES (ranging from $400 to $2000 per kilowatt), estimated at $1000 per kilowatt for GES.

2.3 Electromagnetic method

The electromagnetic ES method defines the accumulation of energy in the form of an electric field or a magnetic field. A current-carrying coil generates ES based on the magnetic field. Practical electrical ESTs include electrical double-layer capacitors, ultra-capacitors, and superconducting magnetic energy storage (SMES). The first type includes electric–capacitor super caps, with a very high-capacity

capacitors. They are also known as supercapacitors. They are specially designed to give high power density (over 1000 W/kg), longevity (>100.00 cycles), and relatively high efficiency (in general over 80 %); the second type is magnetic–super conducting magnetic energy storage (SMES), systems that are also an electromagnetic method of ES. They utilize a magnetic field created by the flow of direct current. SMES systems are involved in many applications, such as power quality at the customer or generator side, voltage control, reactive power compensation and power grid transient stability [8]. For completeness, the flowchart of electromagnetic methods in ESTs is reported in Figure 2.6.

Figure 2.6: Flowchart of electromagnetic methods in ESTs, [8].

2.4 Thermodynamic method

The thermodynamic method is one of the methods for ESTs. It deals with storage, transformation and energy transfer. It involves technologies of thermoelectric, compressed air, adiabatic CAES and thermal heat.
The thermoelectric technology is built on the concept of TES, which is utilized by thermodynamic cycles. The temperature variation circulates between hot and cold thermal storage to drive thermal energy to convert it into electricity eventually.
CAES systems have already been presented as mechanical method, but they can be classified also as thermodynamic one because after being heated, the compressed air drives gas turbines, effectively releasing the stored off-peak electricity. Thermal energy may be stored by elevating or lowering the temperature of a substance (i.e. altering its sensible heat), by changing the phase of a substance (i.e. altering its latent heat) or through a combination of the two. Both TES forms are expected to see extended applications as new energy technologies are developed. TES is the temporary storage of high- or low-temperature energy for later use. Examples of TES are the storage of solar energy for overnight heating, of summer heat for winter use, of winter ice for space cooling in summer and of the heat or cool generated electrically during off-peak hours for use during subsequent peak demand hours. Solar energy, unlike fossil fuels, is not available at all times. Even cooling loads, which nearly coincide with maximum levels of solar radiation,

are present only after sunset. TES can be an important means of offsetting the mismatch between thermal energy availability and demand. ES in the form of sensible heat changes appears very promising for the high-temperature storage of large quantities of energy at fossil-fired power plants. Oil will likely be used as the storage medium for this type of system. Among these categories, Pumped Thermal Energy Storage (PTES) and Integrated thermal energy storage systems (IT-ESS) are included and will be deeply explained in the following chapter.

2.5 Chemical method

The chemical approach to Energy Storage (ES) represents a critical and highly adaptable method, encompassing both thermochemical and chemical application-based techniques. Thermochemical processes rely on a variety of fuels including solar fuel, solar cells and hydrogen. Conversely, chemical application-based techniques involve products such as methane, hydrogen and carbon dioxide.
The thermochemical stores thermal energy through chemical reactions; in this storage, two or more combined components are then separately stored in a chemical compound that breaks down through heat and split components; then, the parts are reassembled in a chemical compound and heat energy is released during high-demand periods. The storage capacity is the thermal energy that is released. However, between demand and supply, thermochemical takes a long time and it is well-suited to generating electricity. The efficiency of this technique ranges from 75% to nearly 100% and thermochemical materials are among the densest in all storage mediums. Solar fuel is a viable energy source from thermochemical methods. It is a synthetic fuel made from water and carbon dioxide using the energy of sunlight; the production involves several reactions. Instead, the solar energy can be utilized to produce hydrogen by water electrolysis using solar-generated electricity and by direct solar water splitting
On the other hand, the methods used to apply chemicals differ from thermochemical methods. Indeed, chemical ones possess higher energy density as compared to present battery technologies. Additionally, they have a longer discharge duration and can be preserved for any time span. The chemical application methods can also be used as raw materials for the chemical industry, direct electricity production and the transportation sector as a replacement fuel.

2.6 Hybrid methods

Hybrid methods for Energy Storage (ES) are engineered to surpass the capabilities of individual ES devices, catering to the demanding requirements of both high energy capacity and rapid response times. One such hybrid ES system is

the battery-supercapacitor hybrid ESS, engineered to deliver a sustained high power density over extended cycles while also offering rapid and efficient energy discharge. These properties render it an attractive solution for enhancing the longevity of electric vehicle (EV) batteries.
Additionally, the combination of battery-battery capacitor hybrids serves to create high-powered buffers suitable for industrial and transportation applications. These hybrids can function as energy output devices themselves or be integrated with various electrochemical batteries, boasting minimal internal resistance and exceptionally high output power.
Fuel cell capacitors find utility in Energy Management Systems (EMS) for ES devices, playing a pivotal role in the conversion of renewable energy interactions with power grids and microgrids.
Lastly, supercapacitor fuel cells are engineered for high power ratings, making them well-suited for mitigating load fluctuations and adept at withstanding voltage variations, rendering them a preferred choice for such applications [8].

2.7 Comparisons

After introducing the whole spectrum of storage technologies, in this section the most common and promising ones are briefly summarized.
The mature large scale energy storage technologies are Pumped Hydro, Compressed Air and Flow Batteries.
One of the most promising ones is the Pumped Thermal Electricity Storage technology; it will be explained in the following chapter, but compared to CAES and PHS, PTES is characterized by higher energy density (110–170 Wh/l or 50–140 Wh/kg), low self-discharge rate (1 %/day), no geographical limitations and small installation footprint. It uses an inert gas as working fluid and cheap storage materials. Therefore, PTES is characterised by low capital costs: 600$/kW and 60$/kWh. It does not suffer of low cycle life like flow batteries and the expected round-trip efficiency (70–80%) and lifetime (25–30 year) are very good. In additions, PTES units can be integrated in fossil-fuelled thermal power plant to reduce cycling operation, fast start up and overnight shut downs.
Further, other in-developing energy storage technologies are GES, LAES and Hydrogen Energy Storage. The first one, as already explained, represents an enhancement of PHS, which does require neither a constant water flow nor a waterfall, but requires stable morphology.
The LAES has the main positive of having air in liquid form, strongly reducing the volume of the storage as compared to CAES.
Finally, Hydrogen Energy Storage is the most convenient way to store off-peak electricity when long term season-to-season storage is needed, but it could be-

come economically feasible around 2030, with high storage capacity and energy density.
Table 2.1 collects both mature large-scale energy technologies (PHS, CAES, Flow Batteries) and the most promising ones, with the main positive and negative aspects of each one, according to what has been presented so far.

TECHNOLOGY	MAIN POSITIVES	MAIN DRAWBACKS
Pumped Hydro Storage	- Low self-discharge - Acceptable price - High round-trip efficiency (up to 87%) - Long life (up to 60 years) - High storage capacity - Low response time (few seconds) - Fast start up time	- Low energy density - Need of water availability - Adequate geographical morphology - Pretty high capital costs
Compressed Air Energy Storage	- Low self-discharge - Good start up time - High round-trip efficiency (up to 95%) - Long life (up to 60 years) - High storage capacity	- Adequate geographical morphology - Pretty high capital costs - Fossil fuel consumption
Flow Batteries	- Low self-discharge - High round-trip efficiency - Acceptable cycle life	- Small storage capacity - Poor lifetime (5-15 years) - High capital costs
Gravity Energy Storage	- Good round-trip efficiency (70-80%) - Long life (up to 40 years) - No need for a constant water flow - No need for a waterfall	- Low energy density - Required stable morphology - Pretty high capital costs
Liquid Air Energy Storage	- Low self-discharge - High energy density - Low storage vessel volume - High lifetime (up to 40 years)	- High costs - High response time
Hydrogen Energy Storage	- Low self-discharge - High storage capacity - High energy density - Good lifetime (up to 30 years)	- Low round-trip efficiency (20-50%) - High capital costs (10000 $/kW)
Pumped Thermal Electricity Storage	- Good energy density - Low self-discharge rate - No geographical limitations - Small installation footprint - Cheap storage materials - Low capital costs - High round-trip efficiency (70-80%) - Long life (up to 30 years) - Possible integration in fossil-fuelled thermal power plant	

Table 2.1: Positives and negatives of the main storage technologies

Chapter 3

PTES and IT-ESS technologies

Before analysing the IT-ESS configuration, which is the central part of this work, it is worth to revisit the fundamentals on the PTES technology. Understanding PTES is essential as the IT-ESS configuration can be considered an evolution of this framework.

3.1 The PTES technology

Pumped Thermal Electricity Storage (PTES), also known as Pumped Heat Energy Storage, represents an emerging storage technology tailored for large-scale Energy Storage (ES) applications. PTES operates on a high-temperature heat pump cycle, converting off-peak electricity into thermal energy and storing it within two thermally isolated vessels: one designated as hot and the other as cold. During discharging, a thermal engine cycle is employed to convert the stored thermal energy back into electrical energy. The working fluid utilized is typically a gaseous medium such as air or argon, with electricity stored in the form of sensible heat using economical and solid materials like concrete, gravel, or other common minerals.
In comparison to Compressed Air Energy Storage (CAES) and Pumped Hydro Storage (PHS), PTES boasts higher energy density (ranging from 110 to 170 watt-hours per liter or 50 to 140 watt-hours per kilogram), a low self-discharge rate (1% per day), absence of geographical limitations, and a compact installation footprint. It leverages an inert gas as a working fluid along with cost-effective storage materials, resulting in low capital costs estimated at $600 per kilowatt and $60 per kilowatt-hour. Moreover, PTES exhibits robust cycle life akin to flow batteries, with expected round-trip efficiencies ranging from 70% to 80% and a lifespan of 25 to 30 years. Additionally, PTES units can seamlessly integrate into fossil-fueled thermal power plants to optimize cycling operations, facilitate fast start-ups and enable overnight shutdowns. Given its power rating and storage ca-

pacity ranging from 0.5 to 10 megawatts (or larger) and 0.5 to 60 megawatt-hours (or larger) respectively, PTES is hailed as one of the most promising large-scale energy storage technologies. PTES functions by storing electricity in the form of heat, which can be stored either as sensible or latent heat. Sensible heat storage involves the storage of thermal energy through changes in the storage medium's temperature, while latent heat storage stores thermal energy as the phase change latent heat of certain media. Solid or liquid media are typically suitable for sensible heat storage, whereas media capable of transitioning from solid to liquid or from liquid to vapor are preferred for latent heat storage.
Sensible heat storage utilizing solid media such as concrete, rocks, or sand represents the most cost-effective, safe and straightforward method for storing thermal energy. Irrespective of the heat storage method employed, in a PTES system, off-peak electricity is first converted into heat using a high-temperature heat pump and stored in two man-made tanks, a process known as the "storing phase." Subsequently, the conversion of stored heat into electricity is achieved through a heat engine during the "delivering" or "discharging" phase.
Pumped Thermal Electricity Storage or Pumped Heat Energy Storage can be categorised according to their thermodynamic cycle and working fluid:

- Closed or reversible Brayton cycle;
- Transcritical Organic Rankine cycle with carbon dioxide as working fluid;
- Compressed Heat Energy Storage system.

The Brayton PTES uses a single phase gas such as argon or air and has two reservoirs, the high pressure one and the low pressure one. The electricity is stored as sensible heat; the first large-scale application was firstly proposed by Desrues et al. [14].
As depicted in Figure 3.1, during the charging phase the system works as a heat pump, converting the electricity into thermal energy, that is then stored inside the two aforementioned artificial tanks. Then, a thermal engine is used for the discharging phase, to reconvert the thermal energy back into electricity. The turbomachines used (two pairs of a compressor and a turbine) allow the circulation of a gas in the tanks, following a closed thermodynamic Brayton cycle. As mentioned, the energy is stored in form of a sensible heat and the working fluid is argon. It is important to note the presence of two heat exchangers in the configuration, a cold one and a hot one.
During the charging phase, the gas moves from the high pressure to the low pressure tank. The high pressure one is gradually heated up, whereas the low pressure one is cooled down.
In the discharging period, the gas follows a heat engine cycle. During this phase, the low pressure tank gradually increases its temperature. Both the charging and

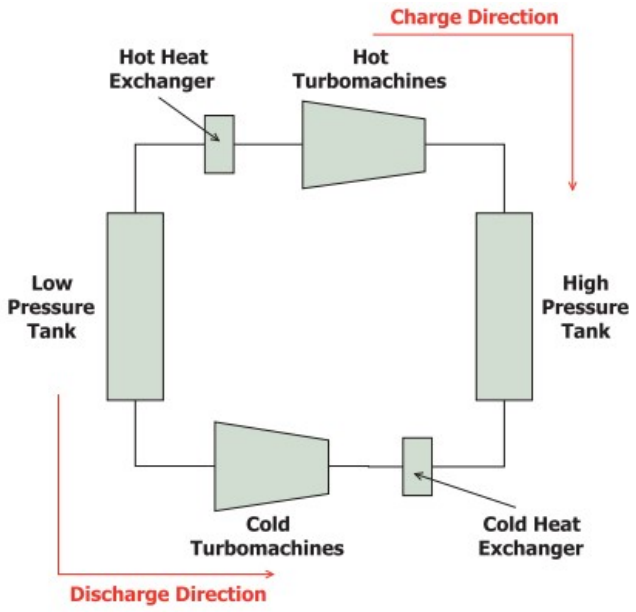

Figure 3.1: Sketch of the plant scheme proposed by Desrues et al. [14].

the discharging periods are considered completed when the temperature of the gas at the outlet of the reservoirs achieves a predefined value, taken as a reference.

In recent studies, Benato and Stoppato [15] presented a PTES configuration (see Fig. 3.2) in which an electric heater is used to convert off-peak electricity into thermal energy, air is used as working fluid and only a heat exchanger is adopted to maintain the expander inlet temperature at its design value. However, during the delivery phase, no heat exchangers are adopted. The system has been designed with the characteristics of commercially available compressor and expander devices.

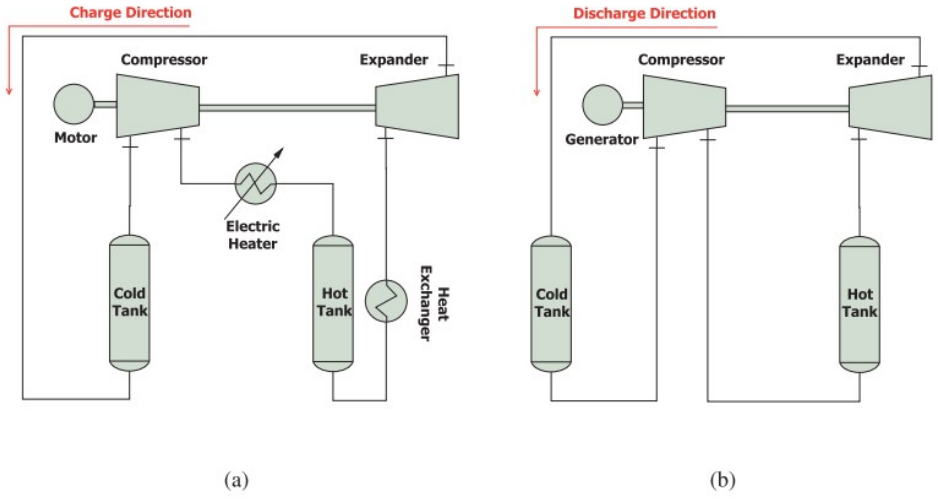

Figure 3.2: Sketch of the plant schemes developed by Benato and Stoppato [15].

During the charging phase, the air enters the compressor and passes through the

electric heater. Upon entering the storage tank, it releases heat to the storage material and then proceeds through the heat exchanger to attain a suitable temperature before entering the turbine. Subsequently, the air flows into the cold storage tank after exiting the turbine. Placing the electric heater after the compressor ensures the maintenance of a constant temperature at the inlet of the hot storage tank. Furthermore, this configuration ensures that the maximum temperature of the cycle is reached at the inlet of the tank. In contrast, in previous configurations where the electric heater was positioned before the compressor, the maximum temperature of the cycle was reached at its outlet, leading to an increase in pressure ratio and device costs. Therefore, with the newly proposed configuration, it becomes feasible to adopt a lower pressure ratio, achieve a high maximum temperature of the cycle and maintain acceptable costs and heat transfer area.

On the other hand, during the delivery phase, the air exiting the compressor enters the hot storage tank where it is heated. Subsequently, the air undergoes expansion through the turbine and is then injected into the cold tank, where it is cooled. During this phase, the heat exchangers are not required, resulting in a reduction in plant costs.

The second configuration related to the pumped thermal energy storage systems has been proposed by Mercangöz et al. [16]. In this work, the authors observed that the typical arrangement of PTES systems requires large storages. Thus, they proposed a new configuration in which a transcritical CO_2 cycle is adopted, with the scope of increasing the efficiency of the plant. Morandin et al. [17] analysed different CO_2 transcritical cycle in order to study their optimization.

Compressed heat energy storage configurations have been proposed by Steinmann [18]; it has a system proposed based on the conventional steam Rankine cycle; during the charge, the water at low pressure is evaporated using the heat coming from a low temperature source such as a heat pump or a refrigeration cycle. After the compression process, the high pressure steam releases its energy in a thermal storage reservoir; then, in this storage, the steam is condensed and the condensate is cooled down to the saturation temperature of the evaporation process. During the discharging process, the heat released by the storage system is used to generate steam used to feed the steam turbine. After the expansion process, the steam is condensed.

3.2 The IT-ESS technology

Seen the urgent need to develop and install new large-scale energy storage systems, Benato and Stoppato [19] proposed a new storage unit that uses air as working fluid and stores electricity under the form of sensible heat.

This new technology is referred to as the Integrated Thermal Electricity Storage System (IT-ESS), and it plays a central role in the presented work. Components found in existing fossil fuel thermal power plants, such as gas turbines, electric generators, step-up transformers, transmission lines, and others, can be utilized to construct IT-ESS plants. Consequently, integrating the storage unit does not require additional overcapacity, revitalises underutilized units and ensures the fulfilment of the urgent need for network flexibility, particularly in terms of load leveling. This aspect is crucial for the effective integration of renewable sources into the energy sector.
Prior to delving into the system's description, it is essential to emphasize that, since this is an open cycle in both charge and discharge modes, the chosen working fluid, which also serves as the heat transfer medium, is air. Utilizing air as a heat transfer fluid ensures the utilization of a readily available, abundant, non-toxic and non-flammable medium.

The charging scheme, as sketched in Fig. 3.3, is made up of a fan driven by an electric motor, a heat exchanger, an electric heater and a man-made tank. An air filter is also placed before the fan intake section. Throughout solar and wind

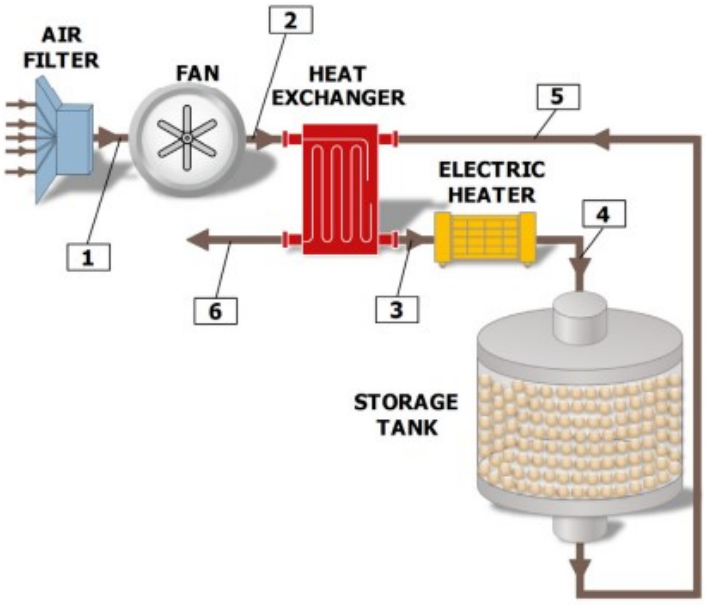

Figure 3.3: IT-ESS charging scheme [19].

power stations high production hours and low load request or in periods characterized by excess power production, the IT-ESS is managed in storing mode. Using the excess electricity to boost the electric motor which in turn drives the fan, the ambient air at atmospheric temperature and pressure is sucked and filtered before entering the fan. Then, the fan increases the gas pressure (process

1–2). The pressurized air passes into a heat exchanger (process 2–3) and, then, into the electric heater where it is heated up: this component acts as a conversion device where the excess electricity is converted into heat (process 3–4). The hot air exiting the electric heater (condition 4), enters the storage tank, heats up the storage material contained into the reservoir and exits (condition 5) at a lower temperature. The air at condition 5 flows across the heat exchanger (process 5–6) and, finally, it is thrown out into the environment. Note that, if the air temperature in point 5 is higher than the one in point 2, the heat exchanger powers up and the air which leaves the tank heats up the one exiting the fan; otherwise the heat exchanger is bypassed. In heat exchanger bypass condition, point 2 matches with point 3 while point 5 coincides with point 6.

Conversely, during high power demand periods or hours when solar and wind power generation is poor, the IT-ESS is managed in production mode using the plant layout depicted in Fig. 3.4. In this case, the IT-ESS is built up with an

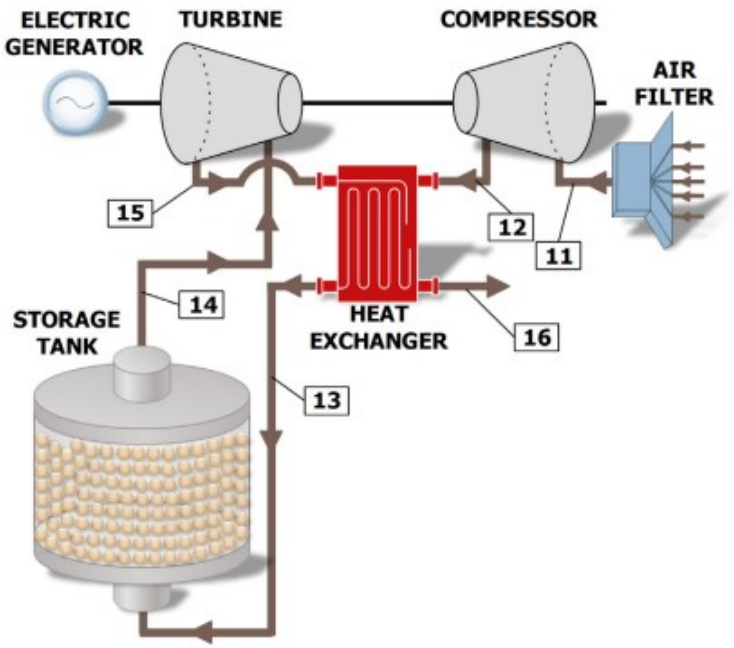

Figure 3.4: IT-ESS delivering plant arrangement [19].

air compressor, a heat exchanger, a storage tank, an air turbine and an electric generator. Upstream of the compressor intake section, an air filter is mounted. Ambient air is sucked, filtered and, then, compressed by the compressor (process 11–12). The compressed air flows throughout the heat exchanger (process 12–13), enters the storage tank and, being the reservoir storage material at high temperature, air is heated up because the previously stored heat is used in this phase to increase the heat transfer fluid temperature. The hot and pressurized air at condition 14 enters the air turbine and expands. Being the air compressor, the air

turbine and the electric generator mechanically coupled on the same shaft, the air expansion generates mechanical power which is, on the one hand, partially used to drive the compressor and, on the other hand, converted into electrical energy by means of the electric generator.
In this approach, surplus electricity stored as sensible heat within the IT-ESS during periods of low demand is subsequently converted back into electrical energy during peak demand hours or when required. Downstream of the air turbine, a heat exchanger is positioned to recover exhaust heat when the temperature at point 15 exceeds that at point 13. Consequently, through this recovery unit, less energy is drawn from the storage reservoir, leading to an extension of its duration. Otherwise, the heat exchanger is bypassed.

As previously elucidated, the aforementioned storage configuration facilitates the straightforward transformation of an existing thermal plant utilizing gas turbine technology into an Energy Storage System. This transformation involves merely replacing the combustion chamber with a sensible heat storage tank.

The plant is engineered to store electricity as sensible heat, which, among sensible, latent, and chemical heat storage methods, represents the most straightforward and cost-effective approach, particularly when employing a gaseous medium as the heat transfer fluid and when constructing large-scale electricity energy storage systems. Practically, storing electricity as sensible heat involves elevating the temperature of the storage medium. This type of storage is widely used and established in various applications such as power production (e.g., solar thermal units), building heating and cooling (e.g., hot water storage), or industrial processes (e.g., glass furnace regenerators). However, it represents a novel approach for large-scale electricity storage setups.

One of the most important components of such a system is the tank; according to [19], it is designed to operate at high temperature, shall be cylindrical in shape, constituted by an upper and a lower plenum and a chamber and vertically arranged.
In Fig. 3.5, a drawing of the tank is reported, showing that air flows from the top to the bottom of the storage reservoir during charging phase while, in delivering mode, the flow is reversed. The distinctive feature of a sensible heat storage tank, as proposed in [20], is that the chamber must be filled with a solid material packed loosely to allow the heat transfer fluid to circulate through the storage material, thereby heating it up or cooling it down. Additionally, arranging the tank vertically helps prevent buoyancy-driven instability of the thermal front. Typically, the storage material comprises spheres of aluminum oxide. The primary criterion for selecting the storage material is to opt for inexpensive, non-flammable, and non-toxic materials. Furthermore, these materials must exhibit favorable thermal properties such as thermal diffusivity and conductivity.

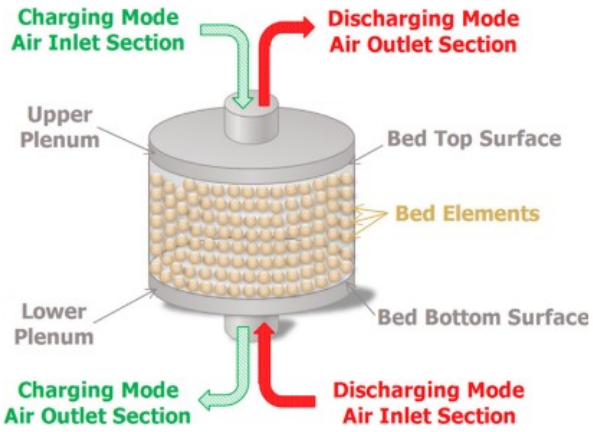

Figure 3.5: Tank's structure [19].

The reasons why this technology is considered one of the most promising ones are explained in the following. The ideal characteristics of a storage technology are: maturity, long lifetime, low cost, high density, high efficiency and environmental friendliness while a large-scale energy storage technology is a system able to store quantity of energy higher than 100 MWh. Meeting all these criteria with only one type of storage technology is still nowadays unrealistic.

Comparing an IT-ESS with Pumped Hydro Storage (worldwide nearly 99% of the installed large-scale energy storage capacity is based on PHS), it is immediately possible to note that the former does not require a particular morphology of the installation site as in the case of the latter, because the storage reservoir is a man-made tank; similar considerations can be drawn also for the specific geological foundation of the underground caver of a CAES plant, where the potential energy of pressurized air is stored; even worse, if the required fossil fuel stream in a CAES plant is taken into account, highlighting a non negligible environmental impact, as compared to IT-ESS.
Furthermore, the low-cycle life of a battery storage plant is not an issue in thermal plants, as well as the self-discharge, being the storage reservoir well insulated. Finally, also compared to other emerging technologies, it must be stated that IT-ESS does not suffer of safety problems and can be commercially available very soon.

Both technologies presented in this chapter are part of the thermodynamic method for the storage of electricity as sensible heat; however, some differences among them are relevant: the PTES unit operates in a closed-cycle, adopts nitrogen as working and heat transfer fluid, needs two storage tanks and the electricity is converted into heat using the compression process. In the IT-ESS plant, there is a unique storage tank which operates at high temperature, the cycle is an open one, air is used instead of nitrogen and the excess electricity is converted into

heat using an electric heater and not by the compression process. One storage reservoir instead of two, ensures to reduce the plant cost as well as the choose of air instead of nitrogen. Using the electric heater instead of the compressor to convert electricity into heat, guarantees to easily control and fine-tune the storage tank inlet temperature. It is also fundamental to underline that PTES requires two heat exchangers: one placed before the compressor and one installed before the turbine. Both are used to maintain constant the compressor and turbine inlet temperatures. These heat exchangers are the main source of losses, leading to greater irreversibilities as compared to IT-ESS, where instead heat exchangers are only used to recover the waste heat and improve the system performance.
To sum up, the Integrated Thermal Electricity Storage technology can be adapted to several different morphologies, while ensuring at the same time a good efficiency and a good cycle life; last, but not least, it has generally a low environmental impact.
Together with the reasons explained in previous sections, these are the main motivations underlying this work thesis. Thus, the following chapter provides a comprehensive overview of the system modelling, conducted using Aspen Plus.

Chapter 4

Aspen Plus model

In the previous chapter the fundamental characteristics of IT-ESS technology have been delineated, as well as its advantages compared to both mature and emerging technologies. Therefore, it is of great importance to be able to model and simulate the behaviour of this technology; however, in several previous works present in literature (e.g. [19], [21], [22]) all the components except for the storage tank have been modelled as steady-state devices, but considering that the system will be part of a real electric grid, in which the energy availability and demand change with time, it is necessary to use the axial compressor efficiency map and the Stodola's equation, in order to properly predict the real components off-design characteristics.
To fill this gap, in this work the software Aspen Plus has been adopted. Advanced System for Process Engineering software (ASPEN) is used to model the power plant. It was developed in collaboration between the Massachusetts Institute of Technology (MIT) and the United States Department of Energy [23]. With Aspen Plus, first a steady-state model is created. Different components in its libraries can be connected together to generate the process under investigation. If users are interested in performing a dynamic simulation, they should switch from Aspen Plus to Aspen Plus Dynamics, where it is possible to model the dynamic behaviour of the power plant, adding control systems, dynamic tasks to perform and scripts. In Aspen Plus Dynamics, it is possible to add and remove components, but it is suggested to use Aspen Plus, to do so. In Dynamics, the transient simulation is based on an unsteady solving of non-linear, one-dimensional partial differential equations, described by using mass, momentum and energy conservation principle together with correlations for heat transfer and friction. Thus, Aspen is a process simulation software widely used in the chemical and thermal engineering and related industries, which allows the users to create detailed models of process units to be used both in a steady-state and dynamic operation mode. However, in Aspen Plus library, a component which is able to properly simulate the behaviour of a thermal storage tank is actually missing and that's

why a robust part of the thesis is dedicated to the modelling of this component. Then, the modelled tank will be integrated with the other components of the plant to perform simulations in charging and discharging operation modes.

4.1 Storage tank models

The construction of the storage model has been made through Aspen Custom Modeler, an easy-to-use tool for creating, editing and re-using models of process units, where dynamic, steady-state, parameter estimation and optimization simulations are solved in an equation-based manner which provides flexibility and power; models written in Aspen Modeler products using the Modeling Language can be used as Unit Operation Models in Aspen Plus and Aspen Plus Dynamics. Before explaining how the tank model has been built, it is worth to investigate and thoroughly understand the most used numerical models for storage tanks. In this work, the model by Benato et al. [24] has been adopted and, according to the authors, three main models have been used in literature and all of them can describe accurately the time-varying behaviour of the storage device. Therefore, in the following, prior to delving into the specifics of the construction of the model in Aspen Custom Modeler, these three models are revised in order to evaluate the most important aspects of each of them and to properly understand how the model adopted in this work has been built.

4.1.1 Model by Howell

The model was presented in 1982 by Howell et al. [25]. The packed bed is schematized through different layers (in number equal to N) over the height of the tank L. Inside any layer, the temperature and the pressure are assumed uniform and constant through the bed element. According to this model, the pressure drop in the tank, Δp, can be computed as:

$$\Delta p = C_f \cdot \frac{L \cdot G^2}{d \cdot \rho_f} \tag{4.1}$$

where C_f is the friction coefficient, $G = \dot{m}/A$ is the specific mass-flow rate, $\dot{m}$ is the mass-flow rate, d is the particle equivalent diameter and ρ_f is the fluid density. The fluid temperature distribution along the bed is computed as:

$$T^t_{f,i} = T^t_{s,i} + (T^t_{f,i-1} - T^t_{s,i})^{-\phi_1} \tag{4.2}$$

where ϕ_1 is the ratio of NTU (Number of Transfer Units) to N, number of layers. The temperature of the bed, instead, holds as follows:

$$T_{s,i}^{t+\Delta t} = T_{s,i}^{t} + [\phi_2 \cdot (T_{f,i-1}^{t} - T_{f,i}^{t}) - \phi_3 \cdot (T_{s,i}^{t} - T_{amb})] \cdot \Delta t \tag{4.3}$$

where

$$\phi_2 = N \frac{\dot{m} \cdot c_{p,f}}{\rho_s \cdot A \cdot L \cdot c_{p,s} \cdot (1 - \epsilon)} \tag{4.4}$$

and

$$\phi_3 = \frac{U_i \cdot \Delta A_i}{\dot{m} \cdot c_{p,f} \cdot \phi_2} \tag{4.5}$$

Here, $T_{f,i}$ is the temperature of the i-th fluid layer, while $T_{s,i}$ is the temperature of the i-th bed's layer. The density of the solid material constituting the packed bed is denoted as ρ_s, while $c_{p,s}$ and ϵ are the solid specific heat at constant pressure and the void fraction of the bed, respectively. The time-step, Δt, is evaluated as $\Delta t = (\rho_f \cdot L \cdot A \cdot \epsilon)/(N \cdot \dot{m})$. U_i is the overall heat loss coefficient and ΔA_i is the external area of a layer.
The Number of Transfer Units can be determined as a function of geometric parameters, of the fluid flow rate and specific heat and of the volumetric heat transfer coefficient; in turn, the latter can be computed as a function of Nusselt number, which is obtainable through the correlations reported by Singh et al. [26]. Finally, the friction coefficient C_f can be again calculated according to Singh et al. [26].
The above set of correlations is useful since they provide an algebraic description of a storage tank and they are valid for packing material with a geometry different from the spherical one, only through the sphericity definition. However, this is a very simplified way to describe the behaviour of the tank and this constitutes a limitation in more complex applications or whenever time-accurate details are required.

4.1.2 Model by McTigue

This model follows the suggestion of McTigue et al. [27]. According to the authors, the model is based on a quasi-steady analysis; the equations governing the heat transfer in the reservoirs are integrated in time in order to study and account for the thermal fronts. This is done since the energy and the exergy losses in the storage tanks depend on the time-history of their operation. As highlighted in [27], the main source of losses in the reservoirs are related to the frictional losses and the heat transfer irreversibilities. Since the heat leakages, with a proper level of insulation, are very low, they are not accounted in the model.

The thermal losses are associated to a finite temperature difference between the gaseous working fluid and the storage material. To quantify these losses, the authors considered the model proposed by Schumann for packed beds [28]. The model assumes that the heat transfer is limited by surface effects and the flow is one-dimensional. Accordingly, the fluid and the solid temperature, T_f and T_s, are assumed to obey the following set of differential equations:

$$\frac{\partial T_f}{\partial x} = \frac{T_s - T_f}{l} \tag{4.6}$$

$$\frac{\partial T_s}{\partial x} = \frac{T_f - T_s}{\tau} \tag{4.7}$$

where l and τ are, respectively, the lengths and the time scale, defined as:

$$l = \frac{1}{St \cdot (1-\epsilon) \cdot S_v} \tag{4.8}$$

$$\tau = \frac{\rho_s \cdot c_{p,s}}{St \cdot c_{p,f} \cdot G \cdot S_v} \tag{4.9}$$

where St denotes the Stanton number, defined as $St = h/(G \cdot c_{p,f})$, and Sv is the surface to volume ratio of the solid particles. Other symbols follow the definitions provided in the previous section.

Based on these hypotheses, White et al. [29] proposed an improved version of Schumann's model by introducing variable properties for the solid and the fluid, including momentum and mass continuity equations. Accounting for these contributions, it is necessary to consider the equations governing the heat and mass exchanges that occur in an infinitesimal control volume along with the tank. The latter is expressed as:

$$\delta\dot{Q} = A \cdot \delta x \cdot (1-\epsilon) \cdot S_v \cdot h \cdot (T_f - T_s) \tag{4.10}$$

where h is the superficial heat transfer coefficient. Then, mass continuity, momentum and energy equations (for both fluid, subscript f, and solid, subscript s) in a differential formulation can be expressed as:

$$\epsilon \cdot \frac{\partial \rho_f}{\partial t} + \frac{\partial G}{\partial x} = 0 \tag{4.11}$$

$$\frac{\partial G}{\partial t} + \frac{\partial}{\partial x}\left(\frac{G^2}{\rho_f} + \epsilon^2 \cdot (p - \rho_f \cdot g \cdot x)\right) = -\epsilon \cdot (1-\epsilon) \cdot \tau' \cdot S_v \tag{4.12}$$

$$\epsilon \cdot \frac{\partial}{\partial t}(\rho_f \cdot e_f) + \frac{\partial}{\partial x}(G \cdot h_f) = (1-\epsilon) \cdot S_v \cdot h \cdot (T_s - T_f) \tag{4.13}$$

$$\rho_s \cdot c_{p,s} \cdot \frac{\partial T_s}{\partial t} = S_v \cdot h \cdot (T_f - T_s) \tag{4.14}$$

The particle surface shear stress is represented by $\tau^{'}$, p is the pressure, g is the gravity acceleration, x is the axial coordinate, e_f is the internal fluid energy per unit mass, and h_f is the fluid enthalpy per unit mass. Equations from 4.11 to 4.14 can be solved in a fully coupled way employing a time-marching algorithm combined with a spatial discretisation method.
However, a simplification of this model has been proposed by Schumann; indeed, to reduce the computation effort, the model can be cast in a semi-analytical version, based on the fact that the main terms of the aforementioned equations can be simplified; accordingly, in order to evaluate the time-dependent terms contribution, a correction factor F can be defined, thereby obtaining a semi-analytical model by integrating the Schumann model and accounting for the factor F. A more detailed and complete explanation of this procedure is available in [29].

4.1.3 Model by Desrues

This model follows the description proposed by Desrues et al. [21]; as highlighted by the authors, the transient phenomena play a central and critical role in the system behaviour. The pressure does not remain constant during a cycle and the thermal fronts change, due to the convective heat exchanges and the thermal diffusivity of the materials employed. According to this, the authors proposed a one-dimensional finite volume method for the discretization of the tank.
Assuming constant solid properties as stated by Desrues et al. [21], the equations used to describe the transient phenomenon for the specific geometry are listed in the following.

Mass conservation of the fluid:

$$\frac{\partial(\rho_f)}{\partial t} + \frac{\partial(\rho_f \cdot v_f)}{\partial x} = 0 \tag{4.15}$$

Energy conservation of the fluid:

$$\frac{\partial(\rho_f \cdot T_f)}{\partial t} + \frac{\partial(\rho_f \cdot v_f \cdot T_f)}{\partial x} = \frac{4 \cdot Nu \cdot k_f}{c_{p,f} \cdot (d_h)^2} \cdot (T_s - T_f) \tag{4.16}$$

Energy conservation of the solid:

$$\rho_s \cdot c_{p,s} \cdot \frac{\partial T_s}{\partial t} + k_s \cdot \frac{\partial^2 T_s}{\partial x^2} = \frac{\epsilon}{1-\epsilon} \cdot \frac{4 \cdot Nu \cdot k_f}{(d_h)^2} \cdot (T_f - T_s) \tag{4.17}$$

Finally, the model is closed by the pressure drop constitutive equation and the ideal gas equation of state:

$$\frac{\partial p}{\partial x} = -C_f \cdot \frac{2}{d_h} \cdot \rho_f \cdot v_f^2 \tag{4.18}$$

$$p = \rho_f \cdot r \cdot T_f \tag{4.19}$$

In the above equations, the subscript f refers to a fluid property, as well as the subscript s to a solid one; further, ρ is the density, v the velocity, T the temperature, k the thermal conductivity; also, t represents the time, x the axial tank coordinate, Nu the Nusselt number, d_h the hydraulic diameter, r is the universal gas constant divided by the fluid molecular weight and C_f the friction coefficient.

The calculation of Nu and C_f is needed to properly evaluate the heat transfer coefficient and the pressure drop, respectively. The correlations available in literature separate the case of a microchannels structure from that of a packing of spheres; in this work, only the latter has been considered, thus the interested reader can refer to Desrues [30] for more details. In the following, the correlations for a packing of spheres are reported.
The hydraulic diameter can be determined by the porosity ϵ and the particle equivalent diameter d as:

$$d_h = \frac{\epsilon}{1-\epsilon} d \tag{4.20}$$

The friction factor can be determined based on Ergun equation:

$$C_f = 2 \cdot (A/Re_h + B) \tag{4.21}$$

where A=150, B=1.75 and Re_h, similarly to the hydraulic diameter, is equal to Reynolds number divided by (1-ϵ).
Finally, Nusselt can be calculated from the Wakao and Kaguei correlation as:

$$Nu = 2 + 1.1 \cdot (Pr)^{1/3} \cdot (Re)^{3/5} \tag{4.22}$$

where Pr is Prandtl number, ratio of the product of dynamic viscosity and specific heat to thermal conductivity, while Re is Reynolds number, ratio of inertia to viscous forces.

4.1.4 Model by Benato and Stoppato

The model proposed by Benato et al. [24] (in the following referred to as TES-PD) relies on the formulation proposed by Desrues et al. [21], just analysed in the previous section. Despite the common starting point, the authors improved it by the integration in the TES-PD model of the entire set of parameters that affect the behaviour of the storage tank. These parameters, that are variously missing in the available literature contributions, are the space and time variability of all the thermophysical properties of both fluid and storage material, the overall heat loss coefficient and the solid material effective thermal conductivity. Indeed, the model by Desrues envisages constant solid and fluid properties computed at an arbitrary reference temperature. This is a strong limitation, which often leads to misprediction in the system dynamics and introduction of uncertainties related to the reference state. Moreover, it can not fit the usage of the most advanced storage materials.
Thus, an important enhancement obtained in the TES-PD model is that the authors embedded the update of both the solid and the fluid properties, considering variability layer-by-layer and updating their values during the time-marching procedure as a function of the actual temperature.
Further, the second improvement has been done by considering the overall heat loss coefficient, which is accounted for only by the model by Howell [25] (parameter U_i in Section 4.1.1); indeed, this coefficient can significantly influence the accurate evaluation of a storage tank, especially when accounting for the potential of charging and discharging periods lasting several days, thereby making it a non-trivial factor in assessing its performance.
Under these hypotheses, the model equations are listed.

Mass conservation of the fluid:

$$\frac{\partial(\rho_f)}{\partial t} + \frac{\partial(\rho_f \cdot v_f)}{\partial x} = 0 \tag{4.23}$$

Energy conservation of the fluid:

$$\frac{\partial(\rho_f \cdot T_f)}{\partial t} + \frac{\partial(\rho_f \cdot v_f \cdot T_f)}{\partial x} = \frac{\alpha}{\epsilon} \cdot (T_s - T_f) \tag{4.24}$$

Energy conservation of the solid:

$$\frac{\partial(\rho_s \cdot c_{p,s} \cdot T_s)}{\partial t} + \frac{\partial}{\partial x}\left(k_{s,eff} \cdot \frac{\partial T_s}{\partial x}\right) = \frac{c_{p,f} \cdot \alpha}{1-\epsilon} \cdot (T_f - T_s) - \frac{U_i \cdot C_u}{1-\epsilon} \cdot (T_s - T_{amb}) \tag{4.25}$$

Pressure drop constitutive expression:

$$\frac{\partial p}{\partial x} = -C_f \cdot \beta \cdot \frac{1}{2} \cdot \rho_f \cdot v_f^2 \tag{4.26}$$

Ideal gas equation of state:

$$p = \rho_f \cdot r \cdot T_f \tag{4.27}$$

All the factors in these equations have already been presented in the previous section, except for $k_{s,eff}$ effective thermal conductivity of the solid, T_{amb} ambient temperature, U_i overall heat loss coefficient and the parameters α, β and C_u. The definitions of the latter three depends on the storage material geometry. Since in this work only the packing of spheres will be considered, the equations for that kind of bed are reported.
In particular, the parameters α and β derive from the model described in [21].

$$\alpha = \frac{6 \cdot Nu \cdot k_f}{c_{p,f} \cdot d^2} \tag{4.28}$$

$$\beta = \frac{1 - \epsilon}{d \cdot \epsilon} \tag{4.29}$$

Finally, C_u is equal to $2\pi A^{-1}\sqrt{A\pi^{-1}}$. The remaining parameters are calculated according to the model by Desrues [21], presented in the preceding section.

4.1.5 Model in Aspen Custom Modeler

As previously mentioned, the initial step in modelling the entire system within Aspen Plus involves creating a model for the storage tank, a component that is absent from the software's library. To achieve this, Aspen Custom Modeler has been employed; this subsystem of Aspen Plus allows the modelling of a component by inputting the equations that describe its behaviour in a specific language. Consequently, this section outlines the construction procedure.

The first step involves the definition of the component list, which contains all the components used in the system; in particular, a component list contains two types of information: a list of component names and a list of options associated with these components. Typically this is used to store options for calculating physical properties for mixtures of these components. All blocks, streams and ports have a built-in property called ComponentList; this contains the name of the component list to be used for the block, stream or port. The easiest way to configure the component list consists in using the Aspen property system and adding the components directly from an imported Aspen file.

The second step involves the definition of the ports. A port is used to define what variables will be passed in or out of a model in streams connected to the model.

```
Model Storage_Tank

/*Definition of the components to be used in the simulation*/
Default as ComponentListName; //Air is the only component inside "Default"

/*Definition of ports as inlet and outlet*/
Inlet  as input MoleFractionPort (ComponentList: Default);
Outlet as output MoleFractionPort(ComponentList: Default);
```

Figure 4.1: Definition of component list and ports

As shown in Figure 4.1, for the model of the thermal storage, in the Default component list the sole component is air; if another fluid is used in the model, in the section "Component Lists", "Edit using Aspen Properties", this can be done. In addition, Mole Fraction ports are used, already defined in the software library; the variables within this kind of port are the molar flow rate, the mole fraction, the temperature, the pressure, the molar enthalpy and the molar volume. Thus, in the model, 6 variables need to be calculated at the outlet.

```
Port MoleFractionPort

 Description: "Metric equivalent of an AspenPlus mole fraction port";
 F                 as flow_mol     (Description:"Molar flow rate");
 z(componentlist)  as molefraction (Description:"Mole fractions", 1.0/size(componentlist));
 T                 as temperature  (Description:"Temperature");
 P                 as pressure     (Description:"Pressure");
 h                 as enth_mol     (Description:"Molar enthalpy");
 V                 as vol_mol       (Description:"Molar Volume");

End
```

Figure 4.2: Mole Fraction port

Then, once the components and the ports have been specified, variables and equations to calculate those variables at the outlet can be defined.
First of all, some variable are fixed (i.e. independent variables).

```
/*Definition of fixed parameters*/
z(Default) as molefraction (fixed, value:1);
p      as pressure (value: Inlet.P);
eps    as RealParameter (value: 0.4, Description:"Bed porosity");
A      as area (value:10, spec:Fixed, Description:"Base area in m2");
r      as length (description:"Equivalent diameter bed particles", value:0.05, spec:Fixed);
```

Figure 4.3: Definition of fixed variables

Among the independent variables, the mole fraction is included; essentially, it will be used only to calculate the properties of the air, as shown in the following. Further, since only low flow rate of air (i.e. low velocity) will be considered, a reasonable assumption is that the properties of the air are calculated at the same pressure (in Figure 4.3 it is fixed at the value at the inlet, that is at the outlet of the previous component).
Also geometric parameters are fixed in the model, in particular the void fraction ϵ (an acceptable value can be around 40%), the area and the length of the tank; a total volume of 50 m^3 is considered, given by a base area of 10 m^2 and a height

of 5 m. Finally, r represent the equivalent diameter of the particles of the bed, assumed to be equal to 5 cm.

Then, since the correlations by Desrues [21] will be used for a packing of spheres, the density at inlet conditions and an average value of velocity need to be defined; in this section, also the molecular weight of air has been calculated. An important note is that the flow rate is given on a molar basis (kmol/hr), therefore in order to calculate the velocity from the continuity equation the flow rate must be converted in kg/s by dividing the molar flow rate by 3600 s/hr and multiplying by the molecular weight. Both the density and the molecular weight are calculated by exploiting the function "Procedure", which allows to calculate properties of a certain fluid when the necessary inputs are supplied; in the case of density, the inputs are the temperature, the pressure and the mole fraction, whereas for the molecular weight only the mole fraction is enough.

```
23    /*Calculation of initial density, average air speed and molecular weight*/
24    call (rho_a) = pDens_Mass_vap (Inlet.T, p, z(Default)) Default;
25    v_mean=Inlet.F/3600*MW/A/rho_a;
26    Call (MW) = pMolWeight(z(Default))Default;
```

Figure 4.4: Calculation of density, average velocity and molecular weight

Up to now, the non-distributed variables have been defined. Then, since the equations that will be used contain some distributed variables along the axial length of the tank, a domain of integration and its correspondent distributed variables must be defined. In order to do this, the domain over which performing calculation has been defined (axial length of storage tank: L). This variable ranges between 0 (tank inlet) and 5 m (tank outlet) and is discretized in 60 parts, a value that demonstrates a good trade-off between computational effort and accuracy. As discretization method, which is also used to solve the differential equations, the Backward Finite Difference (BFD1) or the Upwind Biased Finite Difference of the 4th order (UBFD4) can be considered. The software presents also other discretization methods, but for the scope of the model also a First Order of Approximation method, such as BFD1, is accurate (see [24]).

```
26    /*Domain definition for Ordinary Differential Equations*/
27    L as LengthDomain (Length:5, NumSections:1, SpacingPreference: 5/60, DiscretizationMethod: "BFD1");
28
29    /*Distributed variables definition*/
30    d     as Distribution1D (XDomain is L) of dens_mass_vap;
31    T     as Distribution1D (XDomain is L) of temperature;
32    Thot  as Distribution1D (XDomain is L) of temperature;
33    v     as Distribution1D (XDomain is L) of velocity;
34    mu_a  as Distribution1D (XDomain is L) of visc_vap (free, Description: "cP or mPa*s"); /*viscosity*/
35    K_a   as Distribution1D (XDomain is L) of cond_vap(free, Description: "W/m/k"); /*thermal conductivity*/
36    Cp_a  as Distribution1D (XDomain is L) of cp_mol_vap (free, Description: "kJ/kmol/k"); /*specific heat*/
37    Nu    as Distribution1D (XDomain is L) of pos_small (free); /*Nusselt number*/
38    Re    as Distribution1D (XDomain is L) of pos_large (free); /*Reynolds number*/
39    Pr    as Distribution1D (XDomain is L) of pos_small (free); /*Prandtl number*/
40    alpha as Distribution1D (XDomain is L) of pos_small (free); /*heat trasnfer coefficient*/
41    cp_s  as Distribution1D (XDomain is L) of pos_large (free); /*Solid specific heat in J/molK*/
```

Figure 4.5: Domain and distributed variables

As seen in Figure 4.5, the domain is L, which has a length of 5 m and is divided

into 60 parts. Then, all the distributed variables are defined; these will be used in the equations and in particular in the partial derivatives over x, axial coordinate. Since 12 distributed variables are defined, the same number of boundary conditions and of equations are needed to have a square model.

To start with the boundary conditions, in Figure 4.6 they are written for each variable in the node of the domain corresponding to 0, which represents the inlet of the tank.

```
43  /*Boundary Conditions*/
44  T(0)=Inlet.T;
45  v(0)=Inlet.F/3600*28.95/d(0)/A/eps;
46  Call (d(0))= pDens_Mass_vap (T (0) , p, z(Default)) Default;
47  Call (mu_a(0)) = pVisc_Vap(T(0), p, Z (Default)) Default;
48  Call (K_a(0)) = pCond_Vap(T(0), P, Z(Default)) Default;
49  Call (cp_a(0)) = pCp_Mol_Vap(T (0), P, Z(Default)) Default;
50  Re (0)= v_mean* rho_a  * r / mu_a(0) *1000;
51  Pr (0)= mu_a  (0)* cp_a(0)  / MW / K_a(0) ;
52  Nu (0)= 2 + 1.1 * Pr(0) ^ (1/3) * Re(0) ^(3/5);
53  alpha (0) =  6 * Nu (0)* K_a (0)/ cp_a (0)/1000*MW/ r^2 ;/*Heat transfer coefficient*/
54  Thot(0).ddx=0;
```

Figure 4.6: Boundary conditions

Regarding the temperature, it is easy to understand how the value at the inlet is a known variable, equal to the temperature after the heater in the charging operation mode and after the compressor in the discharging one (if the heat exchanger is neglected). The velocity is determined knowing the value of flow rate and density; the latter is calculated through the function "Procedure", already cited previously. In a similar manner, viscosity, conductivity and specific heat are calculated, by inputting the values of temperature, pressure and mole fraction.
The dimensionless numbers are calculated thanks to previously specified variables in the node 0 of the domain, according to [21]. The heat transfer coefficient α is obtained from Equation 4.28.
Lastly, regarding the solid material, the boundary condition for the temperature of the bed T_{hot} is written by assuming zero-gradient conditions, with first-order of accuracy, for the solid's temperature distribution at the tank's inlet, as cited in [24]. The strategy allows modelling the storage material as adiabatic, packing the heat losses in the dispersion coefficient only. For a matter of space it has not been represented in Figure 4.6 the aluminium oxide specific heat calculation: it has been calculated both in node 0 and all the nodes of the domain from a correlation by Shomate; the latter equation holds as follows:

$$C_{p,s} = A + B \cdot T + C \cdot T^2 + D \cdot T^3 + E/T^2 \tag{4.30}$$

where A=102.4290, B=38.7498, C=-15.9109, D=2.628181, E=-3.007551 and T is the temperature of the bed in Kelvin divided by 1000.

Once the boundary conditions are written, the set of differential equations can be added.

First, in a similar way to what explained for the conditions at the node 0 of the domain, the air properties and the dimensionless numbers are obtained. Again, for a matter of space, the calculation of solid specific heat for aluminium oxide according to Equation 4.30 is not reported.

```
57   /*Calculation of air properties and dimensionless numbers*/
58  =for k in [L.Interior+L.EndNode] do
59   Call (d(k))= pDens_Mass_vap (T(k) , p, z(Default)) Default;
60   Call (mu_a(k) ) = pVisc_Vap (T(k), p, Z (Default)) Default;
61   Call (K_a(k)) = pCond_Vap (T(k), P, Z(Default)) Default;
62   Call (cp_a(k)) = pCp_Mol_Vap (T(k) , P, Z(Default)) Default;
63   Re(k) = v_mean* rho_a  * r / mu_a(k) *1000;
64   Pr (k)= mu_a(k)  * cp_a(k)  / MW / K_a(k) ;
65   Nu (k)= 2 + 1.1 * Pr (k) ^ (1/3) * Re (k) ^ (3/5);
66   alpha (k) = 6*Nu (k)* K_a (k)/ cp_a (k) / 1000 * MW / r^2; /*Heat transfer coefficient*/
```

Figure 4.7: Calculation of properties and dimensionless numbers in all the nodes

It is worth remembering that the multiplication by a constant is typically done to have a consistency in the measurement units; such is the case of Reynolds which is multiplied by 1000, being the viscosity in $mPa*s$ as calculated by the software database.

Actually, 3 equations are missing. They are Equations 4.23, 4.24 and 4.25 of the previous section, which represent the mass and energy conservation of the fluid and the energy conservation of the solid, respectively.
They are written in a partly simplified way; in particular, the solid density in the third equation has been assumed as constant and equal to 3900 kg/m^3, due to issues encountered by the software when dealing with solid species. Also, the effective thermal conductivity of the solid has been neglected, as done in previous works present in literature [24]. The value of the tank thermal transmittance U used to account for the heat losses with the ambient has been kept constant at 0.7 W/m^2K. Again, for a matter of space, the screen from ACM has not been reported.

Before evaluating the conditions at the outlet, the initial conditions must be specified. The temperature of the air is assumed to be uniform and equal to the inlet temperature; regarding the tank temperature, the initial conditions are different depending upon the operation mode. In the charging phase, it is assumed to be uniform at the ambient temperature; as an example in Figure 4.8, it is assumed to be around 300 K (or 27 °C). This holds only when considering the initial charging process.

```
74   /*Initial conditions, for charge*/
75   T ([1:L.EndNode]): Inlet.T, initial;
76   Thot([1:L.EndNode]): 27, initial;
```

Figure 4.8: Initial conditions in the charging operation mode

Conversely, in the discharging phase, the tank can be considered at the uniform design temperature, such as in this case at 1000 °C, as shown in Figure 4.9.

This holds only if the tank is completely charged.

```
78    /*Initial conditions, for discharge*/
79    T ([1:L.EndNode]): Inlet.T, initial;
80    Thot([1:L.EndNode]): 1000, initial;
```

Figure 4.9: Initial conditions in the discharging operation mode

Finally, the variables in the Mole Fraction port must be specified at the outlet, in order to act as an input for the subsequent component of the integrated system. Of course, the exit conditions are represented by the values of the variables in the last point of the domain (i.e. at a distance L equal to 5 m from the entrance); in the language of the Modeler, this node is called "EndNode", so the variables are calculated in that point. In particular, the temperature is easily obtained as the value of temperature in the last node; the pressure is assumed to be decreased by 1%, a conservative value for low values of velocity (i.e. lower than 1 m/s). Regarding the flow rate, it is obtained by the continuity equation, as a function of density and velocity in the last node. The mole fraction is constant and equal to 1 all along the tank; the molar enthalpy is calculated through a Procedure and the molar volume it is the inverse of the density multiplied by the molar weight.

```
82    /*Calculation of the properties at the outlet*/
83    Outlet.T=T(L.EndNode);
84    Outlet.P=0.99*P;
85    Outlet.F=d(L.EndNode)*v(L.EndNode)*A*eps*3600/MW;
86    Call (outlet.H)= pEnth_Mol_Vap (T(L.EndNode), p, z(Default));
87    Outlet.V= MW/d(L.EndNode);
88    Outlet.Z=z(Default);
```

Figure 4.10: Calculation of the conditions at the outlet

Since the literature lacks experimental data as well as numerical results obtained with detailed models like the proposal, the model has been compared with a pre-existing and already validated model built in Matlab Environment, as referred in [15]. Therefore, in order to have a kind of validation of the model, in the following a comparison between the ACM and the Matlab temperature profiles obtained are presented in the charging phase first and in the discharging phase then, as an example.

First of all, the parameters used in the Matlab algorithm are itemized:

- The inlet conditions of pressure, temperature and mass flow rate, respectively. The inlet conditions are related to the behaviour of the other devices of the system. In particular, the inlet temperature to the tank, during the charging phase, depends on the electric heater. In the simulations performed the inlet temperature is maintained constant and is assumed equal to 1000 °C. This choice is connected to the maximum feasible temperature

with the material used in the storage tank. In the discharging phase, the inlet temperature is the one of the compressed air, so it is above the ambient temperature.

- Height L, volume V and number of layers of the tank N. The number of layers of the tank describes the degree of detail of our calculations, and is the number of subdivisions of the tank of thickness equal to $\Delta L = L/N$. For each subdivision the algorithm proceeds with the balances of mass and energy. In our simulations, the number of layers assumed is equal to 60, that can be considered a good compromise between quality of the results and speed of the algorithm used in the description of the system. The choice of the volume and of the height of the tank is related to the different management strategies of the system and on the limit related to the Nusselt number, ad described in [26].
- Ambient and design temperature.
- Density of the storage material and its thermal conductivity (this last parameter is assumed equal to 0 W/(m · K) [24]). Its specific heat has been derived from NIST database.
- Thermal transmittance of the storage tank.
- Equivalent diameter of the storage particle and their sphericity (that is assumed equal to 1).

4.1.6 Charging operation

Parameter	**Value**
Tank height	5 m
Area	10 m^2
Number of layers	60
Void fraction	0.4
Diameter bed particles	0.05 m
Tank thermal transmittance	0.7 W/m^2K
Air flow rate	8 kg/s
Pressure	10 bar
Initial tank temperature	27 $°C$
Design temperature	1000 $°C$
Ambient temperature	15 $°C$

Table 4.1: Parameters used in the simulation during a charge operation

In Table 4.1, the most important parameters used in the simulations to compare the codes in the charging operation mode are listed. At time $t = 0$ s the tank is at a uniform temperature of 27 °C and it will be heated up by the flow of 8 kg/s of air at 1000 °C and 10 bar. In real charging operations, the pressure is just slightly above the atmospheric value. To perform a proper comparison, the temperature profiles of the tank after 1 hour and after 5 hours are shown.

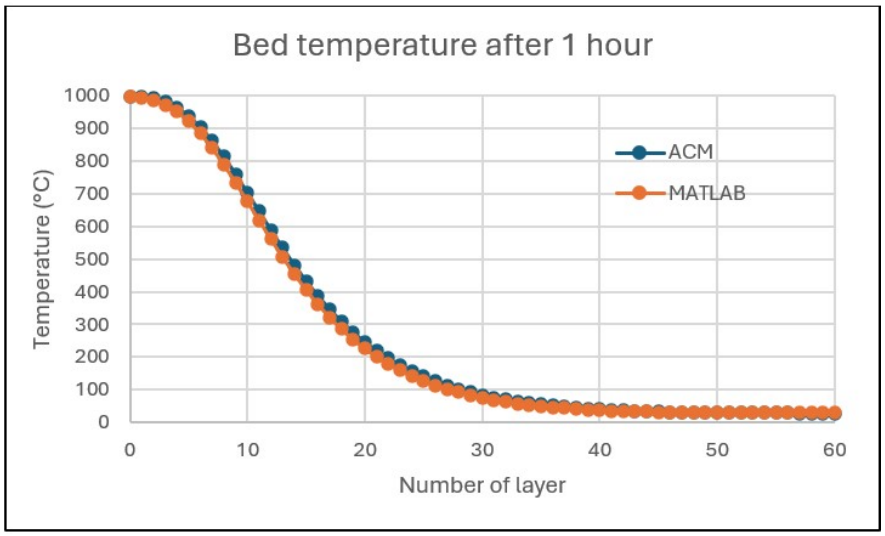

Figure 4.11: Bed temperature after 1 hour

In the plot of Figure 4.11, it can be seen that the temperature trends are similar; the discretization method used may influence the distribution of the temperature along the tank. In Matlab Environment a first-order generalised upwind finite difference method was employed to compute the first spatial derivatives, whereas in ACM a backward finite difference method was used. However, this dissimilarity does not constitute a particular issue to be solved because the focus is not on the temperature distribution inside the tank, but primarily on the outlet temperature of the air, since a complete system will be analysed in the following sections, not just an individual component.

On the other hand, after 5 hours the profiles of temperature are approximately overlapped, being the only difference the temperature distribution between nodes 45 and 55. Instead, the outlet temperatures are in both cases close to 700 °C. After 5 hours, nearly 70 % of the tank has reached the temperature of the air which is flowing inside. The temperature distributions can be seen in Figure 4.12, highlighting that, being very difficult to heat up the last layers of the tank, typically a distribution like the one shown is considered sufficient for a charging process.

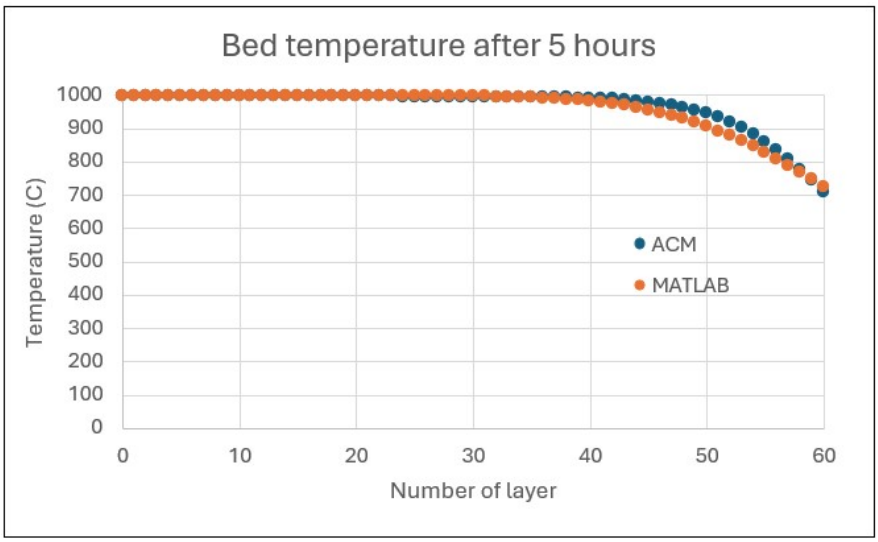

Figure 4.12: Bed temperature after 5 hours

4.1.7 Discharging operation

In Table 4.2, the most important parameters used in the simulations to compare the codes in the discharging operation mode are listed.

Parameter	**Value**
Tank height	5 m
Area	10 m^2
Number of layers	60
Void fraction	0.4
Diameter bed particles	0.05 m
Tank thermal transmittance	0.7 W/m^2K
Air flow rate	8 kg/s
Pressure	10 bar
Initial tank temperature	1000 $°C$
Inlet air temperature	380 $°C$
Ambient temperature	15 $°C$

Table 4.2: Parameters used in the simulation during a discharge operation

In this case, it is assumed that the tank has an initial uniform temperature equal to 1000 °C; again a flow rate of 8 kg/s of air flow inside the tank; however, differently from before, the air has a lower temperature than the bed, thus it will be heated up, while cooling down the bed, in order to have a hot flow of gas at 10 bar, which will drive the turbine to generate mechanical and electric power. It is worth to note that the air is not at ambient temperature but it has a larger temperature due to the compression. In a similar way to what has been done

in the previous section, the plots of bed temperature after half an hour and five hours will be presented. Of course, the temperature of the bed will tend to the temperature of the air which is flowing inside (in this example 380 °C, discharge temperature of a compressor with an isentropic efficiency equal to 72%). The other parameters are all the same as before; in particular, the volume of the tank is assumed again to be 50 m^3 and it is discretized in 60 layers over a length of 5 m.

In Figure 4.13, after 0.5 hours, just the first 15 layers of the bed have started the cooling process, while in the remaining ones, it is not yet started, being the air very hot because of the heat exchange with the first layers. As before, the differences in the profiles are tight, highlighting a good modelling of the tank behaviour. The gap between the bed temperatures in the 2 profiles is lower than 10 °C in the first layers, whereas approximately null in the remainder.

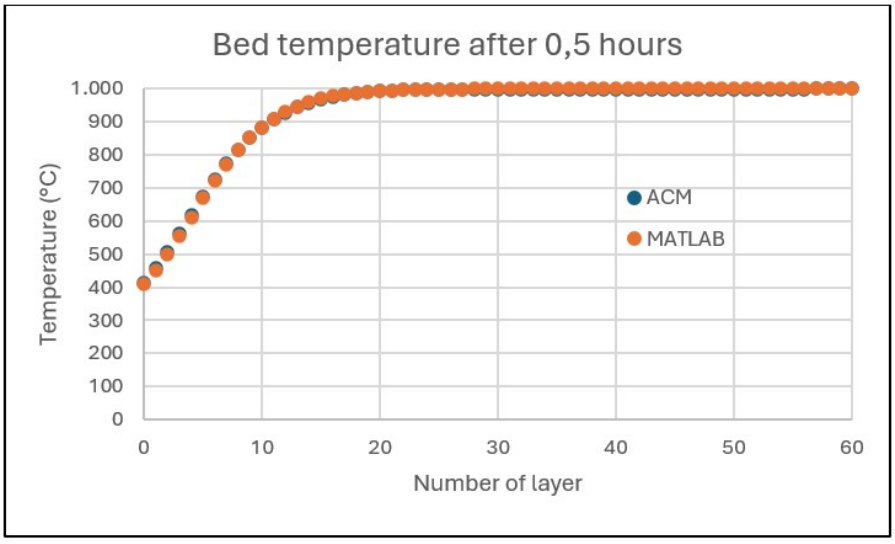

Figure 4.13: Bed temperature after 0.5 hours

A good accuracy of the ACM model is shown also in Figure 4.14, in which the temperature profile after 5 hours is represented.

With a good approximation, the first 40 layers of the bed have already reached the temperature around 380 °C, while the last ones are still at a higher temperature. However, in this case, ACM slightly overestimates the temperature of the last 10 layers of around 20 °C. Again, this may be due to the different discretization method, which distorts the calculations also close to the outlet zone. However, for the proposals of this work to describe the behaviour of the entire system, this difference is not so relevant and will not be investigated in a deeper detail.

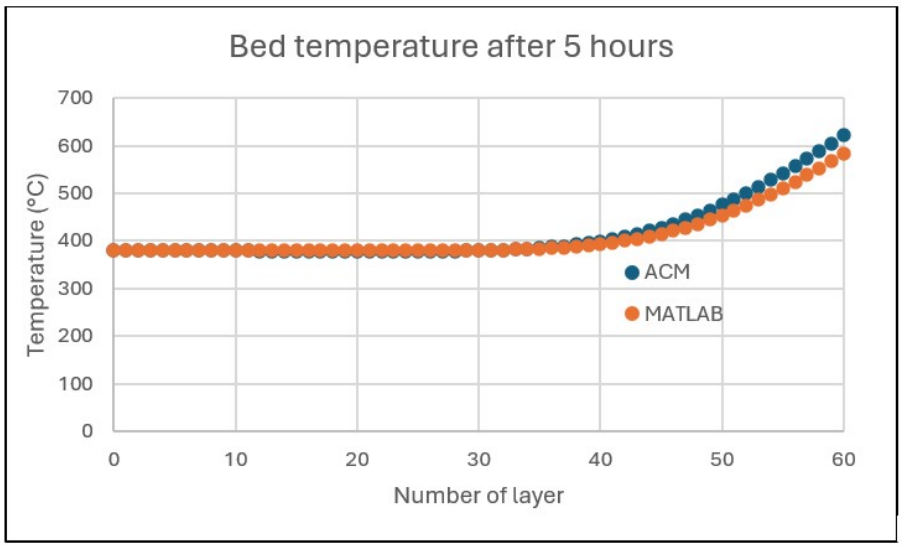

Figure 4.14: Bed temperature after 5 hours

4.2 Overall system model

In order to employ the model for process design simulation, it has to be transferred to the AP environment. To perform this task, it is necessary to have installed, besides ACM and AP, a Microsoft C++ compiler and to follow the procedure explained in ACM User Guide (AspenTech, 2003):

- From the Exploring Simulation pane, right click on the model to export and pick the Package Model for Aspen Plus/HYSYS wizard. Explore the various options available through the wizard for configuring the install package and accept the default options.
- When ACM asks whether you want to install the package, hit "Yes" and follow the installation instructions.
- The model has been exported to AP. In order to appear in its Model Library, open AP and from the "Library" menu, pick "References" and check the box next to "ACM Models".
- A new pane called "ACM Models" will appear in the model library palette, from which the customized model can be selected for the use in any flowsheet.

4.2.1 Charging operation mode

In the charging phase, the scheme of the system is the one shown in Figure 3.3. In the simulations performed in Aspen Plus Dynamics, the air filter component is

meaningless, while the heat exchanger is neglected to simplify the system, but still having good accuracy. Therefore, there are only 3 components which represent the whole system: a compressor, an electric heater and a thermal tank.

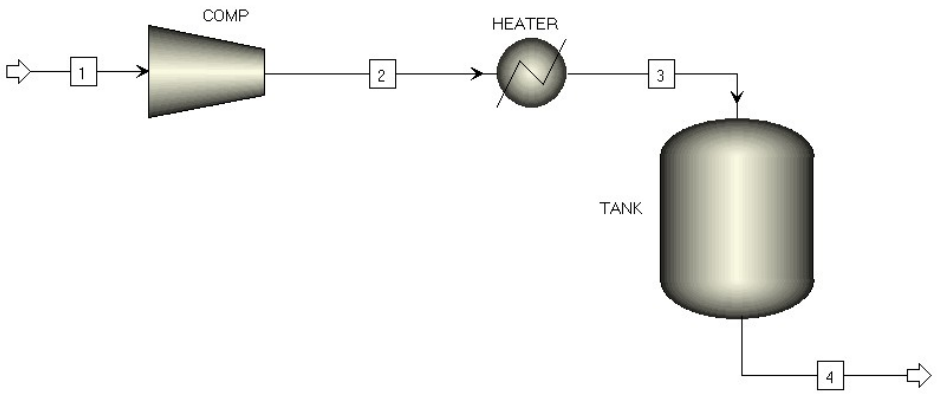

Figure 4.15: Charging operation mode in Aspen Plus Dynamics

Atmospheric air entering the compressor in stream 1 is compressed to a value of pressure which is able to push the flow inside the tank and exit from the latter at atmospheric pressure; thus, in stream 2, air has slightly larger values of pressure and temperature than ambient conditions. In the electric heater air is heated up to 1000 °C; however, the design temperature can vary depending on the choice of the designer. If pressure drops in the pipes and in the heater are neglected, air at 1 bar and 1000 °C enters the tank, where it is cooled down by rejecting heat to the storage material, which conversely heats up. This process of heat exchange can last up to the point in which air and storage material achieve the same temperature. In the chart of Figure 4.12, it can be seen that around 40 of the total 60 nodes of the domain have reached the design temperature after 5 hours of simulation. Since an increase of temperature also in the last nodes is more and more difficult and takes longer as most of the nodes reach the design temperature, typically the tank is considered to be fully charged after 5 hours at constant air flow at 1000 °C, as done in previous works, such as [31].

4.2.2 Discharging operation mode

On the other hand, in the discharging phase, the sketch of the system is the one depicted in Figure 3.4. Again, in Aspen Plus Dynamics, the air filter component is meaningless and the heat exchanger is neglected for a simplicity of simulation. During high power demand periods or hours when solar and wind power generation is poor, the IT-ESS is managed in production mode, like the one shown in Figure 4.16; indeed, this operation mode is also known as delivering arrangement.

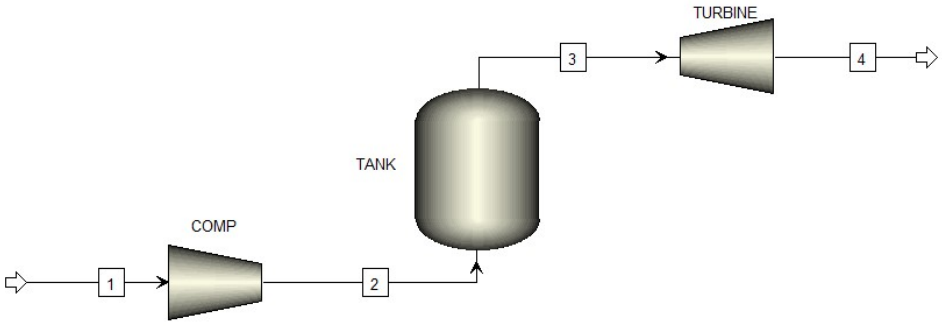

Figure 4.16: Discharging operation mode in Aspen Plus Dynamics

Air at atmospheric conditions enters the compressor, where achieves a pressure around 10 bar, even though this value can be changed depending on optimization and safety conditions. In this case, air is colder than the tank ambient (ideally the storage material can be considered at a uniform temperature of 1000 $°C$) and thus heats up while cooling down the bed. Therefore, air at high temperature and pressure drives a turbine, producing mechanical power at the shaft; the latter is used partly to drive the compressor, being connected at the same shaft, and partly converted into electric energy by means of an electric generator, reconverting the excess stored energy during low demand hours again into usable electricity.

Chapter 5

Dynamic simulations

As a first step in the dynamic simulations, a constant flow of air may be considered. Then, in the following sections, a sensitivity analysis of a few parameters will be developed and then a hint for the adoption of a control system will also be mentioned; the latter solution is more realistic because, as aforementioned, this storage will be part of an electric system, in which the energy availability and demand change with time; further, considering that the heater and the compressor will be driven by a renewable energy source, such as photovoltaic or wind, the intermittency of these kind of sources leads to a strong dynamic behaviour of the system and thus a need of a powerful control system.

5.1 Design conditions

5.1.1 Charging process with uniform tank temperature

A mass flow rate of air equal to 5 kg/s enters the compressor at 15 °C and 1 bar. The compressor has a polytropic efficiency of 85% and a mechanical one of 95% and discharges the flow of air at 1.03 bar in order to compensate the subsequent pressure losses in the heater and in the tank; indeed, this value is enough to push the air flow inside following components; considering a pressure loss of 1% both in the heater and in the tank, the air leaves the system at atmospheric pressure. The heater heats up the air up to 1000°C and releases it into the packed bed, which stores the energy in form of sensible heat and is assumed to be at a uniform initial temperature of 27 °C.

With these operating parameters, the compressor brake power is constant because the flow rate of air does not vary over time, as well as the remaining working parameters, such as inlet temperature and pressure. Its brake power is equal to 15 kW.
On the other hand, the heater has a much larger duty required to heat up that

Working parameters	Value
$\dot{m}_{air}$	5 kg/s
T_1	15 $°C$
p_1	1 bar
Compressor operating shaft speed	3000 rpm
Polytropic efficiency	0.85
Mechanical efficiency	0.95
Heater outlet temperature T_3	1000 $°C$
Heater pressure drop	1%
Tank pressure drop	1%
Initial tank temperature	27 $°C$

Table 5.1: Fixed variables in an initial charging process

flow rate, but again it is constant over time and equal to 5345 kW; in percentage, the ratio of compressor power to required duty is 0.3%, thus the former might be even neglected in any calculation for the efficiency; this result is important and obvious, as the compressor just have to allow the flow to reach the tank and so only compensates the pressure losses, which however are small, being the velocity only slightly larger than 1 m/s, while Reynolds number ranges between 500 and 1350 depending on air temperature, which in turn affects the viscosity, while the product density-velocity is approximately constant. The aforementioned values are represented in Figure 5.1, where in green the duty of the heater prevails on the blue line of the compressor brake power.

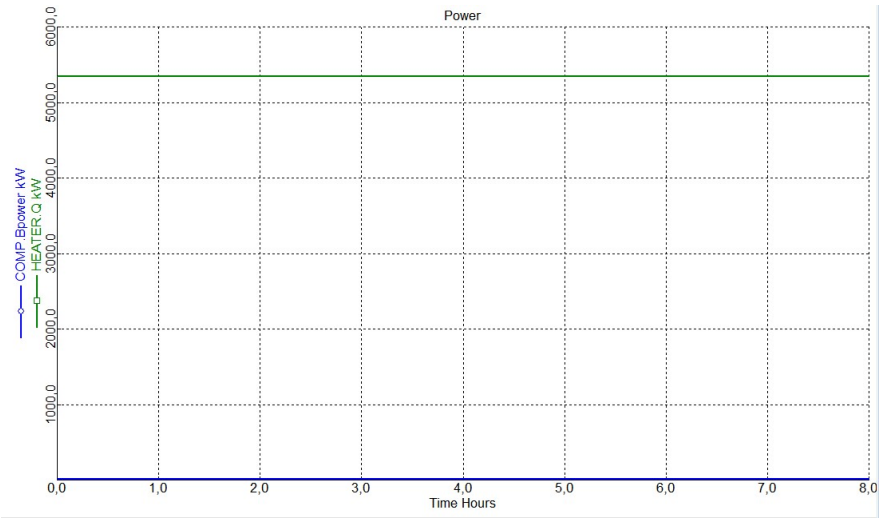

Figure 5.1: Compressor power and heater duty in a charging process

In Table 5.2, all the relevant thermodynamic conditions calculated by Aspen Dynamics are collected. As mentioned, the conditions in stream 1 are fixed and

equal to environmental ones; in stream 2, the air has been compressed by a fan at a slightly larger pressure and temperature; in stream 3, a small pressure drop and a high increase in temperature up to 1000 °C are given by the heater, which allows the flow to heat up the tank; at the end, air at nearly atmospheric pressure exits the tank, with a highly variable temperature.

Design conditions	**Charge**
$\dot{m}_{air}$	5 kg/s
T_1	15 $°C$
p_1	1 bar
T_2	17.9 $°C$
p_2	1.03 bar
T_3	1000 $°C$
p_3	1.02 bar
T_4	See Fig. 5.2
p_4	1.01 bar

Table 5.2: Temperature and pressure of the streams

As seen in Table 5.2, an interesting trend to analyse is the one of T_4, which is the temperature at the outlet of the tank and hence of the system. It is highly variable during the dynamic simulation and in particular, considering that at the beginning the tank is assumed to be uniformly at 27 °C, first the air flow heats up the area close to the entrance, reaching then the last layers at a lower temperature and thus exchanging less heat with them and delaying their warming-up; in addition, an important factor to be considered when analysing the performance of such a system is that part of energy could be directly recovered by the exiting airflow, especially towards the end of the charging operation mode, when it has a high energy content.
In Figure 5.2, this concept is represented; indeed, after 3 hours, the last layer (i.e. the outlet temperature) is still approximately unchanged in temperature; then, a sharp increase affects the trend and in one hour the temperature has increased by 70 $°C$, in the subsequent hour by 100 $°C$, and so on. At the eighth hour, assumed to be the end of the charging process, it has reached 710 $°C$; however, the maximum achievable temperature by the last layer is around 990 $°C$, but this would require at least 2 hours more and its cost-effectiveness should be carefully evaluated.

Remembering again that a time of 8 hours has been considered to have a nearly complete charge of the tank, it is worth to report the temperature field at the end of the process, where it is clearly shown that the very last portion of the tank has not achieved the design temperature. Informations about the outlet

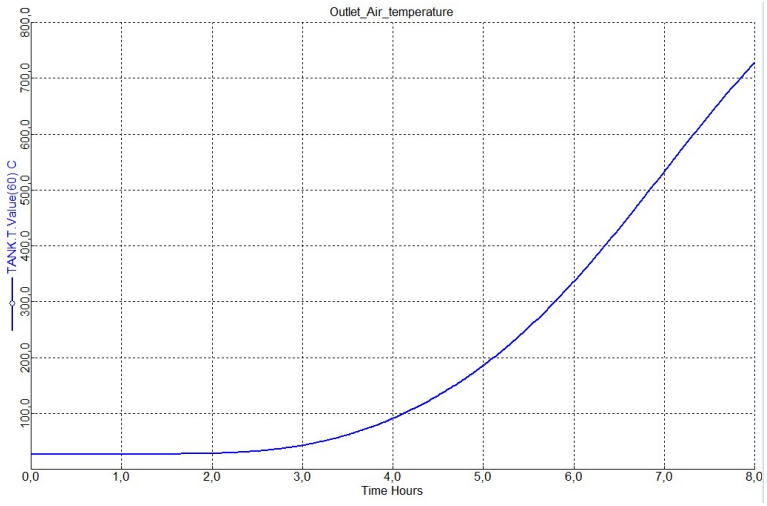

Figure 5.2: Outlet air temperature trend over time

air temperature have been already given in the above paragraph, whereas the remaining layers are shown in Figure 5.3. This will be the starting point of the subsequent discharging operation.

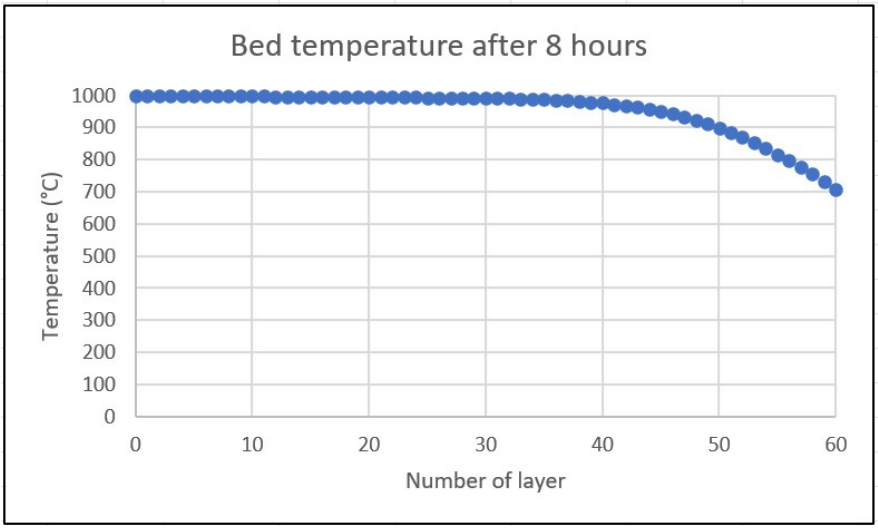

Figure 5.3: Bed temperature distribution at the end of the charging process

Around 40 layers out of 60 have reached the design temperature (slightly below 1000 $°C$), whereas the last ones have a decreasing trend, which leads to an outlet temperature of 710 °C, as seen in Figure 5.2.

5.1.2 Discharging process

As the charge operation has been considered as concluded, starting from a temperature inside the tank uniform and roughly corresponding to the ambient conditions, a possible assumption is that in a few minutes a discharging process

occurs, thereby keeping the same temperature distribution inside the tank as in Figure 5.3 as starting conditions of the new operation. A necessary important assumption is that between the two processes there is not enough time to change the temperature distribution in the packed bed and to vary the values of temperature. Thus, the initial conditions of the simulation are different from what has been adopted so far, when a uniform temperature was always assumed, also in Chapter 4 with the validation of the model. The sketch of the system is the one represented in Figure 4.16. Table 5.3 collects the fixed parameters in the discharging process, which starts with a not uniform tank temperature field.

Working parameters	Value
$\dot{m}_{air}$	5 kg/s
T_1	15 $°C$
p_1	1 bar
Compressor and turbine operating shaft speed	3000 rpm
Polytropic efficiency	0.85
Mechanical efficiency	0.95
Compressor pressure ratio	10
Tank pressure drop	1%
Exhaust turbine pressure p_4	1 bar
Initial tank temperature	See Fig. 5.4

Table 5.3: Fixed variables in discharge design conditions

In a discharging phase, the air flow is reversed with respect to the charging process, that is the gas flows from the bottom to the top of the tank; thus, the temperature distribution curve must be flipped, leading to the one shown in Figure 5.4, where layer 0 is the air inlet and layer 60 the air outlet.

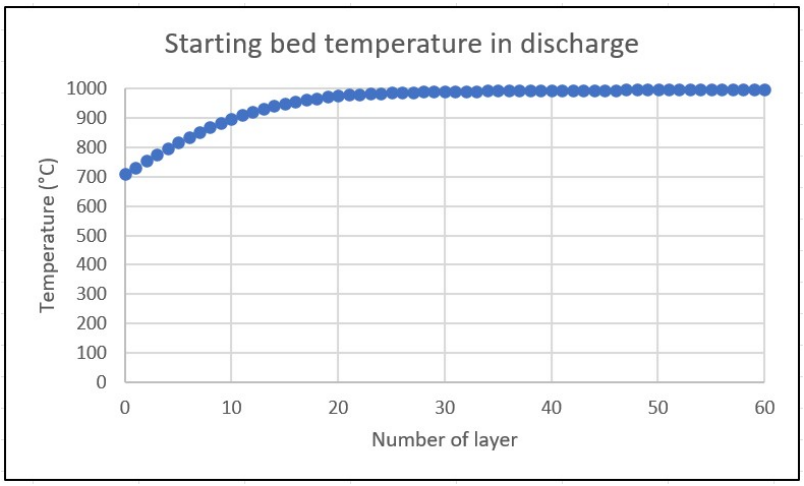

Figure 5.4: Bed temperature distribution at the starting of the discharging process

Since the goal of such a system is to recover the electricity which was stored in form of sensible heat inside the tank, it is effective to work until the turbine-generated power exceeds the compressor-absorbed power. The latter is constant and equal to 1650 kW, used to compress 5 kg/s of air at 10 bar; this compression releases the flow at 326 $°C$ into the tank; thus, the tank can be cooled down to around 326 $°C$ as minimum temperature. One of the most relevant parameters is the temperature at the outlet of the tank or, in other words, at the inlet of the turbine; this is typically referred to as TIT, which stands for turbine inlet temperature. This parameter strongly affects the output from the turbine, being the pressure and the flow rate constant.

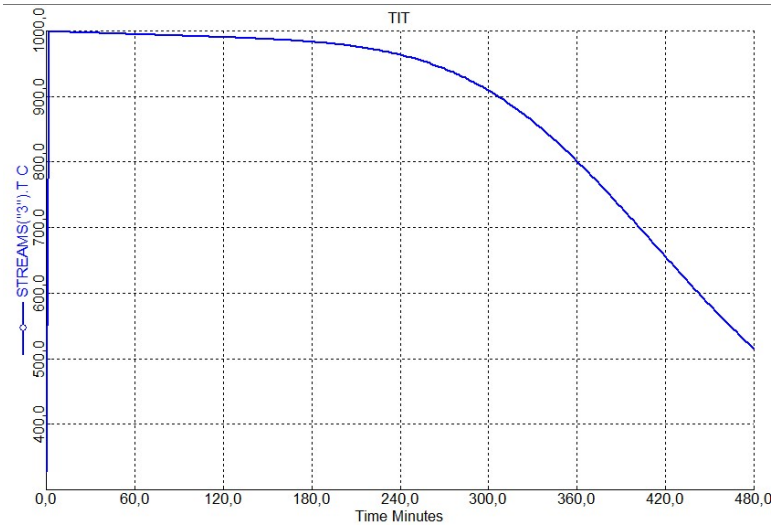

Figure 5.5: Turbine inlet temperature trend over time

Its trend is represented in Figure 5.5 and shows a non-linear behaviour; indeed, at the beginning of the dynamic simulation it is assumed to be at 25 $°C$ to approximate ambient conditions; as soon as the air starts to flow inside the tank (the temperature of the latter is shown in Figure 5.4), it immediately increases to around 1000 $°C$, then it is approximately constant for several minutes and finally decreases, first slightly, then considerably; such a trend can be explained by thinking to the initial tank temperature distribution: first, the air heats up in the first layers while cooling down the bed; then, the hot air flowing inside the tank is further heated up by the last layers, which initially are at the design temperature. To help in understanding and explaining this concept, in Figure 5.6, the tank temperature distributions after 6 minutes (i.e. at the beginning), after 2 hours and after 6 hours are reported.
As evident, the tank is cooled down in the first layers, which already after a few minutes have decreased down towards a lower temperature; thus the air being already at a high temperature extracts less heat from the subsequent layers, which are at high temperature longer. After 6 hours the temperature of the

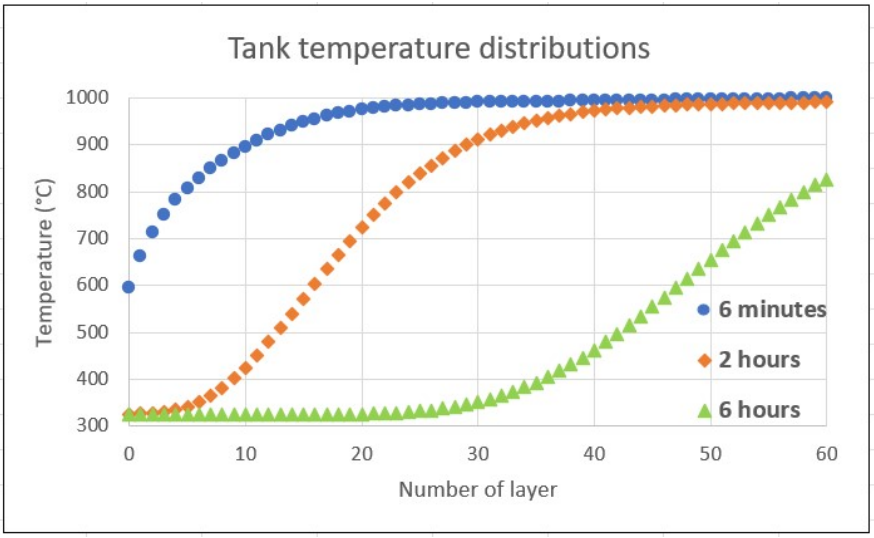

Figure 5.6: Tank temperature distribution at different times

sixtieth later has decreased; indeed, the air can extract less heat from the tank initial layers and thus is not capable of achieving high temperature, leading to a sharp decrease in the value of TIT, like the one shown in Figure 5.5 after 4 hours.

Following this idea, in Figure 5.7, the turbine power is represented; the maximum power is achieved at the beginning, where the curve has a relative maximum point, and it is equal to roughly 2900 kW; then, it tends to decrease as TIT decreases, with the same trend of the latter, first slowly, then much steeper.

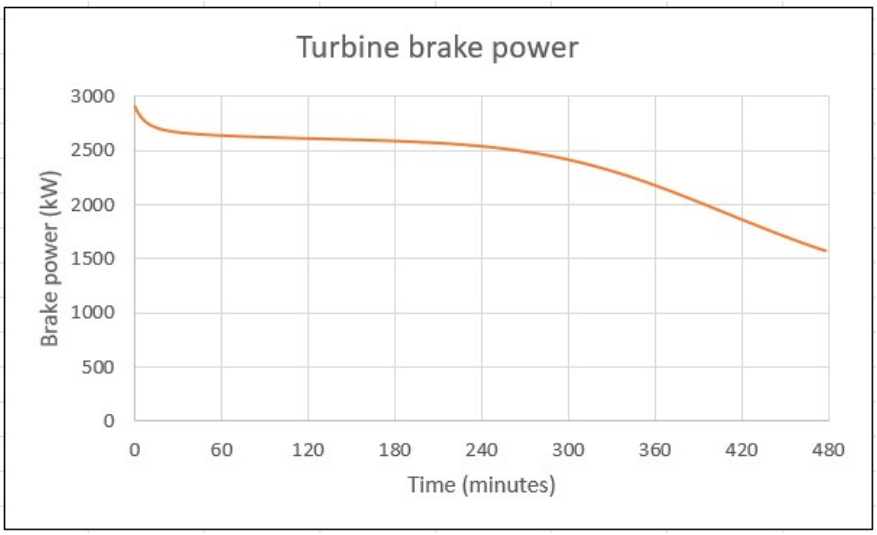

Figure 5.7: Turbine generated power over time

During the simulation, the turbine power ranges from 2900 kW at the beginning to 1650 kW at the end of the process.
Accordingly, in Figure 5.8, the net power is represented: it is the difference be-

tween the generated power by the turbine and the absorbed power by the compressor; the latter is constant over time, as the system is analysed under design conditions, whereas the latter has the trend which has been already explained and is reported in Figure 5.7. It is worth to run the system until the net power value is larger than zero, that is if the turbine power is larger than the compressor one. In this example, the system should be stopped after 460 minutes, as evident by the figure, because then the net power starts to be negative and thus the system absorbs power, instead of releasing.

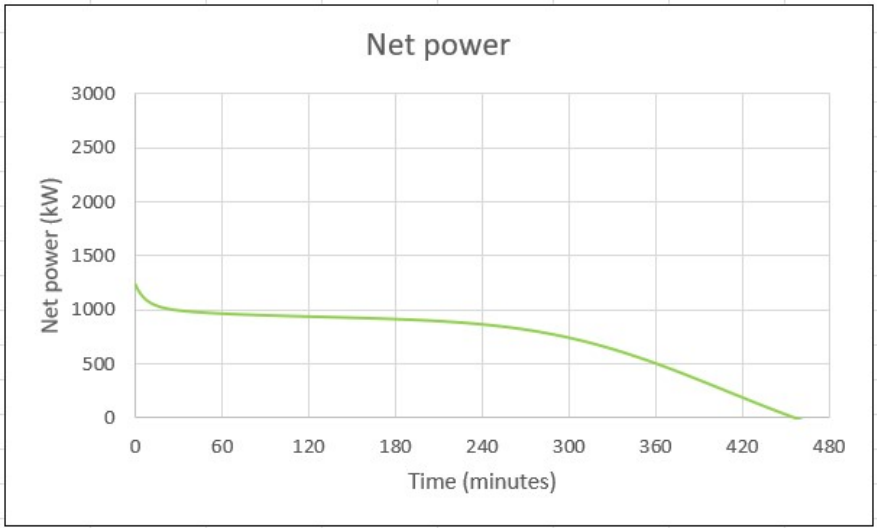

Figure 5.8: Compressor and turbine powers over time

Regarding the performance of the system, it is important to note that, being the tank in the charging phase considered initially at 27 $°C$, the efficiency of first charge and discharge is very poor, around 13%, with an electric input in the charging phase equal to around 45 MWh and an output in the delivering arrangement of 5.7 MWh; the stated value isn't strictly a round-trip efficiency because, traditionally, such efficiency requires achieving the same temperature distribution at the end of discharging as at the beginning of charging (with the tank uniformly at 27 $°C$). However, due to compressed air entering the tank at 326 $°C$ during discharging, restoring a 27 $°C$ temperature inside the tank is unfeasible. Consequently, the efficiency is referenced to the initial charge.
Its value is inherently low for two primary reasons. Firstly, a significant portion of energy remains unexploited because during discharging, air enters the tank at 326$°C$, rendering the energy within this temperature range irrecoverable. Secondly, inefficiencies of the system's components contribute to the overall reduction in efficiency.
Moreover, a substantial loss in efficiency occurs in the outlet airflow stream, which could potentially be mitigated by incorporating a heat exchanger in a more comprehensive system design. Thus, for an accurate performance estimation, it's im-

perative to consider, at the very least, the input power during a charging process when the tank's temperature distribution reflects that of a previous discharging process.

5.1.3 Recharging process

As aforementioned, in this second process of charging the initial tank temperature is not uniform; assuming that among the end of the discharging process and the starting of this operation has not passed enough time to change the temperature distribution inside the packed bed, the initial conditions for the temperature distribution are exactly those at the end of the previous operation, that is after 8 hours of air flowing at 10 bar and 326 $°C$; for completeness, in this section the temperature distribution used as initial conditions for the tank is reported in Figure 5.9, remembering again that the flow in the two operation modes are reversed and such is the distribution.

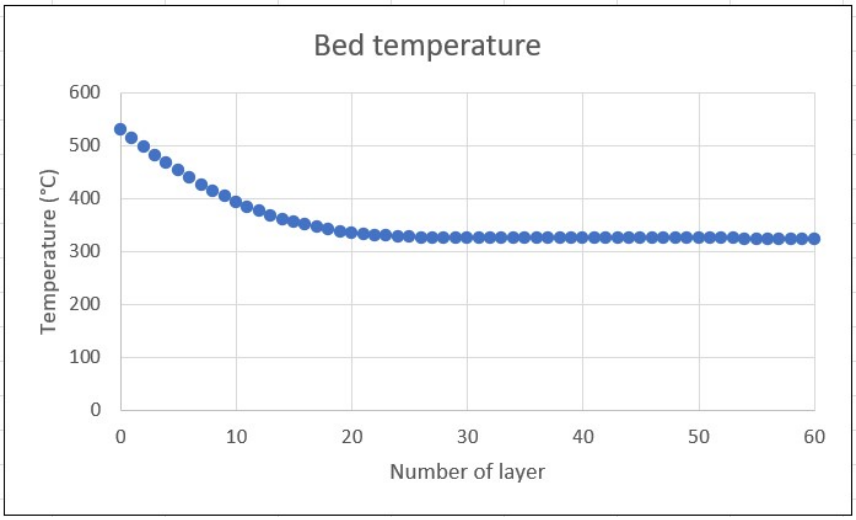

Figure 5.9: Flipped tank temperature distribution at the end of discharging

Again a flow rate of air of 5 kg/s at 1000 °C is used to heat up the tank. In this case less time is necessary to heat up the tank, as in each layer the temperature is greater or equal to 326 $°C$. The trends after 2, 4 and 6 hours are reported in Figure 5.10.
In around 6 hours, nearly the same temperature distribution as the one shown in Figure 5.3 is obtained but with 2 hours less, that is with more than 10 MWh not dispatched; this implies an increase in efficiency with respect to the first charge case up to around 17 %, which is not such a high value, also because in the system the heat exchanger able to recover part of the heat from the air exiting the tank in the charging phase and exiting the turbine in the delivering arrangement has not been considered.

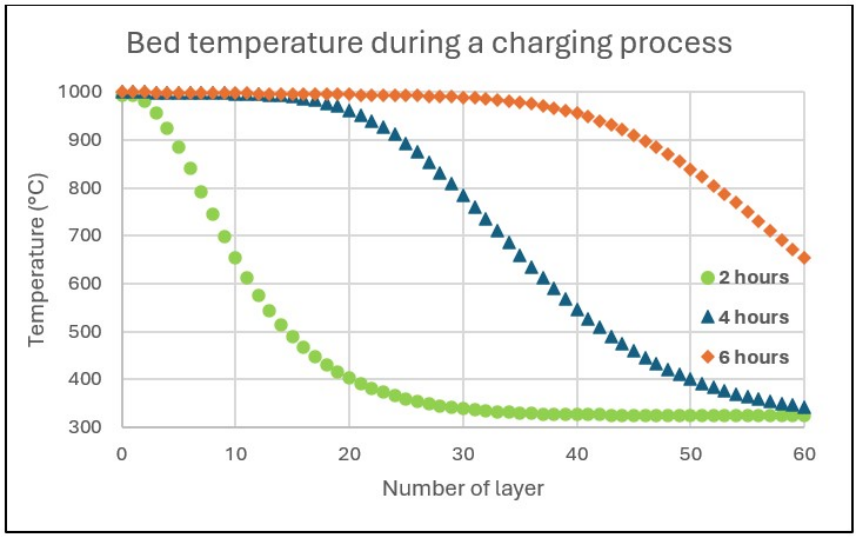

Figure 5.10: Tank temperature distribution in a charging process

Just as an example to understand the latter concept, the air temperature at the exit of the tank during this charging phase is reported in Figure 5.11.

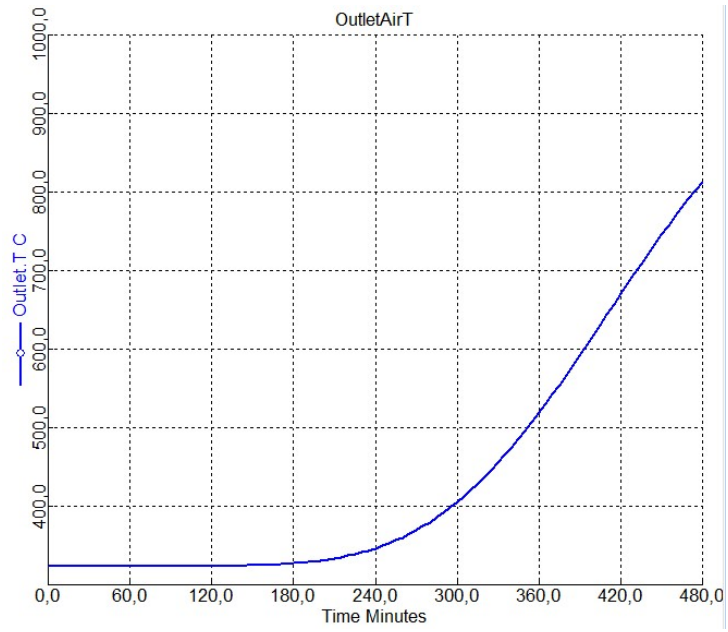

Figure 5.11: Air outlet temperature in a charging phase

The heat content in this airflow is lost, whereas if a heat exchanger was adopted it could be partly recovered by heating the air before entering the electric heater, thus reducing its required power and increasing the overall system performance. The heat exchanger would have a strong positive impact on the system performance from the fourth hour, when the air temperature at the outlet starts to get larger. However, it increases the costs of the plant, thus its cost-effectiveness

needs to be investigated.

5.2 Sensitivity analysis

In the previous section, simulations were carried out with specified values for variables such as flow rate, compression ratio, tank number of layers and size, ambient temperature, and others. Now, it's crucial to examine how alterations in these variables may influence the system's results. This step is pivotal in optimizing the system and understanding the behaviour also in off-design conditions.

Therefore, the following sensitivity analyses focus on the airflow rate, pressure ratio and number of layers, as they are considered the most significant parameters.

5.2.1 Flow rate variation

The air flow rate entering the fan during the charging phase must be decided based on the available power to be rejected at the heater. However, a general consideration, demonstrated in the following with the plots from Aspen Dynamics calculation, is that the larger the flow rate, the larger the power needed to heat up it and the faster the heating up process of the tank.
In previous works (see [31]), the flow rate was varied roughly from 1 kg/s to 7 kg/s. Thus, in the following, a chart presenting the bed temperature distribution after 8 hours in an initial charging process (initial bed temperature 27°C) has been reported in order to understand the influence of the flow rate in the heat exchange process. The independent variables are the same as those seen in the previous section in Table 5.1, except for the air flow rate.

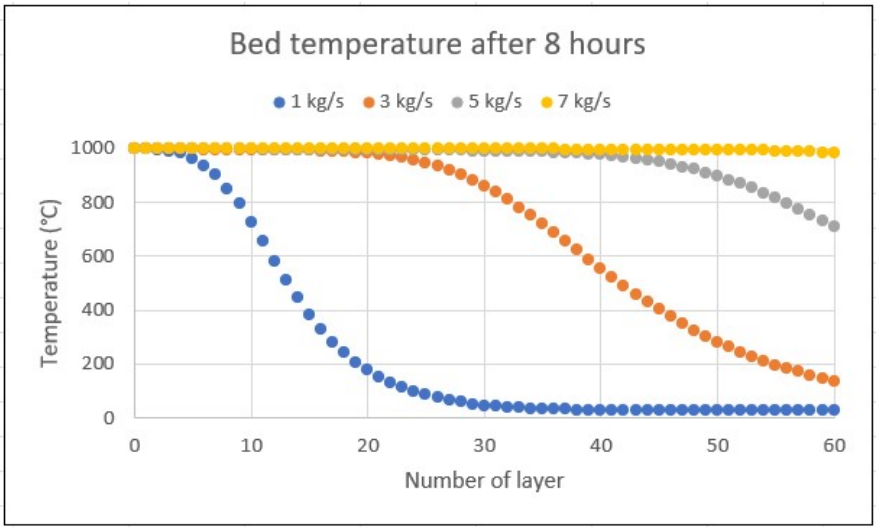

Figure 5.12: Bed temperature distribution with different air flow rates

As evident and expected, a low flow rate results in a notably inefficient heating

process of the tank, also due to the reduction in Reynolds number, consequently leading to a decrease in the heat transfer coefficient. For instance, after 8 hours, with an air flow rate of 1 kg/s, the majority of layers remains at the initial temperature; however, with a flow rate of 3 kg/s, a more satisfactory temperature distribution is achieved. At 7 kg/s, all layers have nearly reached the intended design temperature. Nevertheless, in practical scenarios, it is often not worthwhile to continue operating the system until all layers reach the design temperature. Instead, a temperature distribution similar to that observed with a flow rate of 5 kg/s is typically considered sufficient for the charging process. This is because heating the very last portion of the tank is considerably difficult and not cost-effective. Moreover, considering that higher flow rates result in larger pressure drops, it is essential to note that the fan must exert greater compression on the airflow to overcome these increased pressure drops when the flow rate exceeds 5 kg/s. Consequently, the assumption of constant pressure within the tank becomes less tenable.

The same analysis on the flow rate can be performed both in a discharging process and in a normal charging process. In the former, a reduced value of extracted turbine power is obtained with low flow rates; this is very useful in order to be able to follow the load and thus, when the requests from the grid increase, the flow rate shall increase as well, and vice-versa. To perform such an operation, a control system is required. Similar considerations to the ones shown in Figure 5.12 can be done in a normal charging process (bed temperature different from the ambient one and not uniform).

5.2.2 Compression ratio variation

This analysis focuses on the discharging process, where the compression ratio has a big impact on the performance of the system. A larger pressure ratio causes a greater temperature of the air entering the tank (i.e. at the exit of the compressor), thus less heat is extractable from the tank.

In order to understand the importance of a proper choice of pressure ratio, several simulation have been done while keeping as constant the mass flow rate and all the remaining parameters, except for the compression ratio. Table 5.3 in the previous section contains the same parameters as those used in this specific sensitivity analysis (again, except for the pressure ratio value), remembering that the starting bed temperature in this discharging process is the one obtained at the end of the previous charging operation, shown in Fig. 5.4, as done in Section 5.1.2 with a flow rate of 5 kg/s.

One of the most important results consists in the evaluation of the net power extracted from the system, given by the difference of the turbine generated power and the compressor absorbed one. Figure 5.13 depicts this information: as the

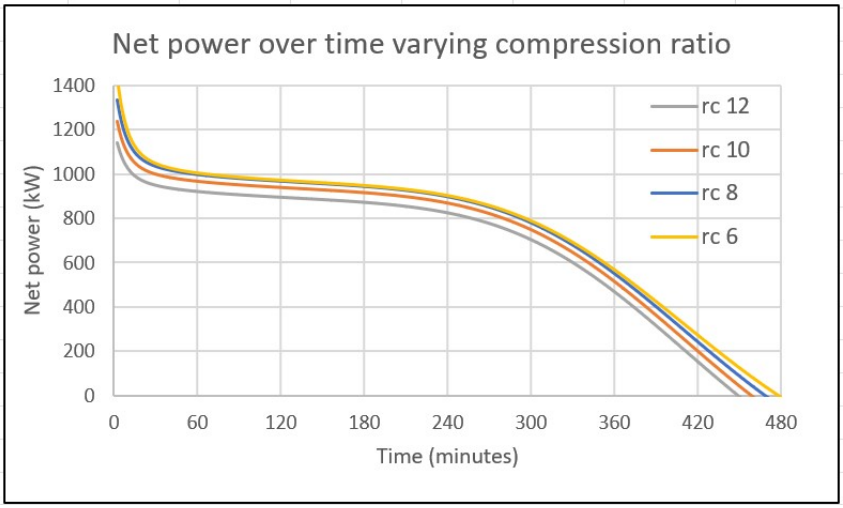

Figure 5.13: Net power trend with different compression ratios

compression ratio increases, the net power decreases. This is due to the compressor's required power increasing slightly faster than the power generated by the turbine as the pressure ratio rises. However, this trend is only applicable within the range illustrated in the figure, from a compression ratio of 6 to 12. Notably, at a pressure ratio of 4, it has been observed that there is a decline in the net power extracted and this is omitted from the chart for clarity. Consequently, the optimal compression ratio, given the above working parameters, falls between 6 and 8, lower than the value utilized in the preceding section. However, with a lower air pressure entering the tank, there is an increase in velocity and thus pressure losses, primarily due to a reduction in density; therefore, an optimization process must consider both of these factors.

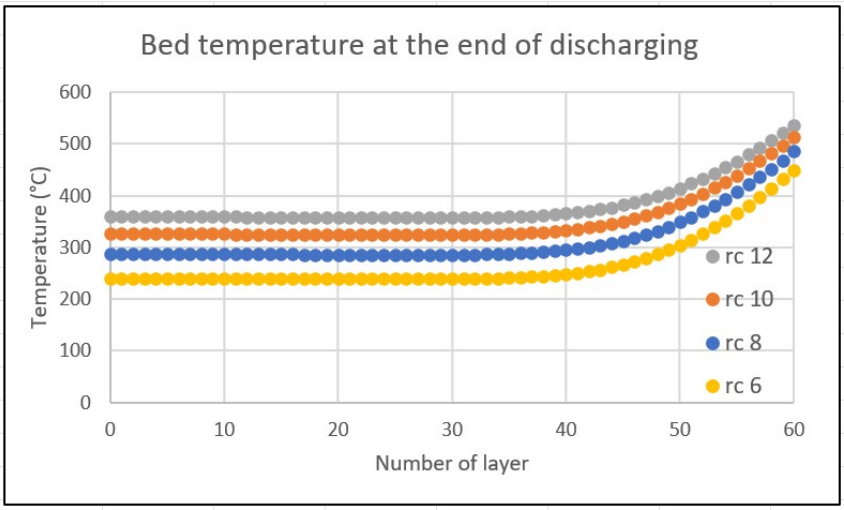

Figure 5.14: Bed temperature distribution with different pressure ratios

Another positive aspect found with a lower pressure ratio is the temperature dis-

tribution inside the tank at the end of the discharging process.
As depicted in Figure 5.14, the higher the pressure ratio, the higher the temperature in each layer of the tank; this is evidently a result of the rising temperature in the compressor as the compression ratio increases. Consequently, air entering at a higher temperature can extract less heat compared to when it enters at a lower temperature. This observation is particularly significant because it means that more heat can be stored during the charging phase if the starting temperature distribution inside the tank is lower.

5.2.3 Variation in number of layers

Regarding the number of layers in the discretization method when describing the behaviour of the storage tank, its choice has been done in order to find a trade-off between the time of calculation and the accuracy of the results.
To understand the choice of this parameter, several simulations have been performed and Figure 5.15 collects a result which allows to compare the different discretization methods, that is the outlet air temperature from the tank in a charging process over time, adopting the same working parameters as previously shown in Table 5.1 for the initial charge.

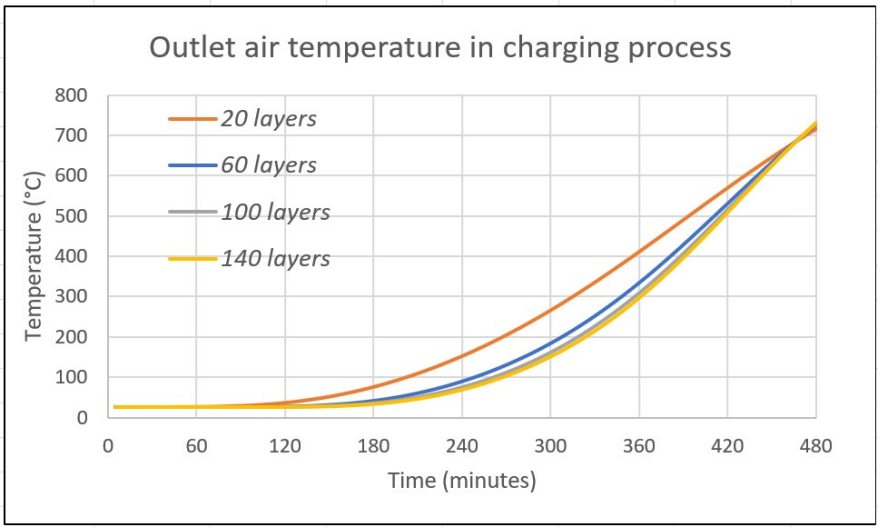

Figure 5.15: Variation in outlet air temperature with different number of layers

Considering a reduced number of layers, such as 20, with each layer having a depth of 25 cm due to a tank height of 5 m, the temporal trends diverge from those observed with a higher number of layers. Conversely, transitioning from 60 layers to 100 and subsequently to 140, the disparities in temperatures at each time step get smaller and smaller. However, in terms of computational time, there is a noticeable escalation in the time required for computation with finer discretization; specifically, there is more than a 50% increase in computational

time for every increment of 40 layers. If a case study requires very time-accurate values, a higher number of layers leads to more accurate results but the computational time increases as well. In the previous simulations, 60 layers have been considered satisfactory to describe the overall behaviour of the storage system. Finally, it is important to state that these calculations have been done with a tank height equal to 5 m; with a taller or shorter tank, the number of layers needed to have an accurate description of the behaviour is larger and smaller, respectively.

5.3 Control system and future works

To enhance the modelling of this storage system, the implementation of control systems is suggested to simulate the real dynamic behaviour. The block PIDIncr in Aspen Plus Dynamics can be used. PIDIncr models a proportional integral derivative controller using an incremental control algorithm, as used in most modern electronic controllers. Key features of PIDIncr include:

- Ideal, series, and parallel algorithms;
- Auto, manual, and cascade operation;
- Optional tracking of the process variable by the set point when in manual mode;
- Optionally when slave controller set to cascade, initialize master controller output to slave controller set point;
- Anti-reset windup;
- Various input filtering options;
- Dead banding;
- Auto-tuning capability;

PIDIncr and PID are both models of PID controllers. They have similar features but are implemented differently. PID uses a positional algorithm to calculate the controller output from the current error and accumulated integral error. PIDIncr uses an incremental algorithm which calculates the change in the output as a function of the error.

The implementation of PIDIncr is closer to that of real industrial controllers, and it models their detailed behavior more closely. In particular there is no bump in the output when you change the tuning parameters during a dynamic

simulation, whereas PID may give a bump in the output. This make PIDIncr better for tuning controllers as a simulation runs.

By means of such a controller, the mass flow rate or any other parameter can be managed in order to properly face the needs of the grid.
As an example, during the charging phase, the energy must be stored but, as well known, the power may not be constant; indeed, typically it is intermittent, such as from photovoltaic or wind, and thus not constantly available and predictable. If a control system is not adopted, the air would not be heated up to the same temperature by the heater (e.g. 1000 $°C$), but it would vary based on the availability of power from the sources. Thus, the importance of a controller is evident: as the power availability decreases, the mass flow rate should decrease as well, and vice versa. Very simply, in Figure 5.16, the linear trend of the electric heater required power is reported versus the mass flow rate; therefore, a control system shall be able to track the curve and adjust the entrained mass flow rate to the available power, instant by instant, in order to have a maximum cycle temperature as constant as possible.

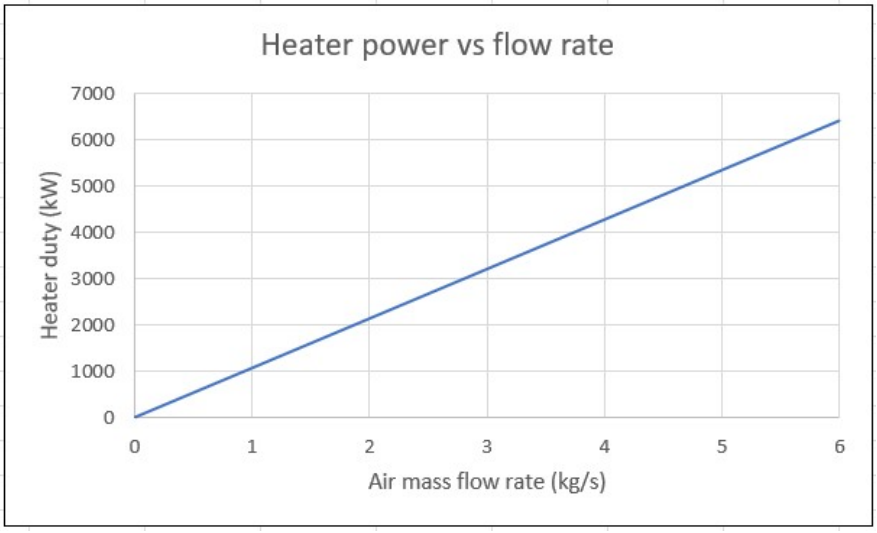

Figure 5.16: Heater duty as a function of air flow rate

An important note is that this required duty has been calculated with the same fixed variables as shown before in Table 5.1. At different environmental conditions, the values may be slightly different; further, when the heat exchanger to recover the heat available in the exiting air is considered, the values are lower, especially towards the end of the charging process, when the air leaves the tank with a high thermal energy content, which is exchanged with the entering air. In conclusion, this simple trend has just been drawn to highlight the importance of a control system in the charging phase; in Aspen Plus Dynamics it can be simulated by means of the aforementioned PIDIncr block, allowing to change manually the input values of available power (for instance, following the production curve of

a PV system) at different hours of a day and getting as controller output automatically the entrained mass flow rate of air. The maximum and minimum flow rates depend on the working ranges of the components and are chosen based on the heat source expected production curve.

Regarding the discharging phase, in real operating conditions, the required power depends on the electric grid demand. Thus, the handled air mass flow rate cannot be generally constant. Furthermore, to properly simulate the behaviour of the system and track the working point of the machines, the compressor efficiency map and Stodola's equation should be implemented in Aspen Plus; this last part can be easily done thanks to the versatility of the software. Actually, a curve to represent the off-design behaviour of compressors and turbines is already present, so it's just a matter of changing the values with the real ones.

As a starting point for future works, in Figure 5.17, a possible control system idea has been reported; in particular, the compressor and the turbine are connected to each other through a work stream to simulate the single shaft. Furthermore, the block PIDIncr, previously mentioned and named "CONTROLLER" in the figure, is used to act as a controller of the air flow; in detail, it gets as input the signal of the power produced to the shaft and gives as output the entrained mass flow rate in the compressor. The former is an input to the system because the required power by the users is an instant by instant known quantity.

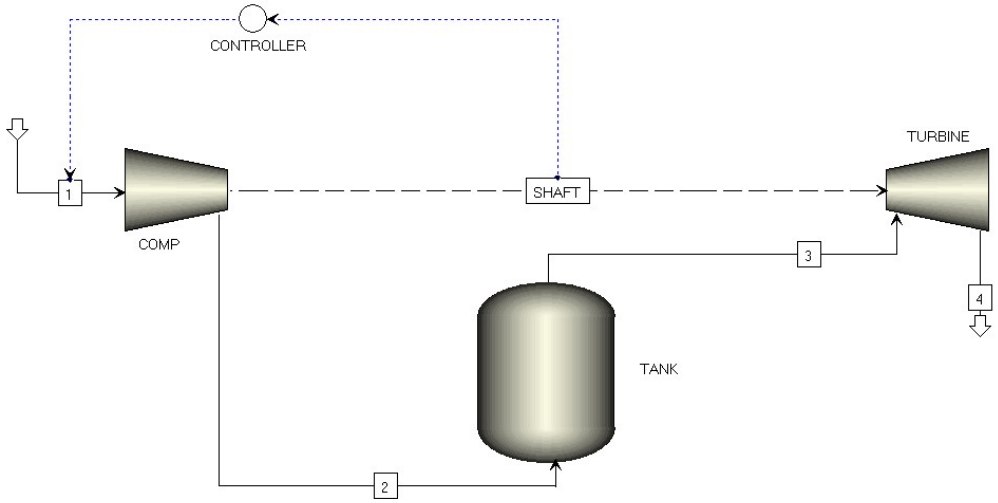

Figure 5.17: Power control system in discharging process

The control system described above requires integration with other controllers for proper implementation and should be considered as a suggestion for future developments. As mentioned earlier, an additional step to improve the model is the incorporation of component curves; in this case as well, initially assuming a constant mass flow rate may serve as a starting point. Accurately predicting the turbine performance entails considering the variations in turbine inlet tempera-

ture and thus in efficiency, which are influenced by the tank emptying process.

In this section, only a few suggestions for the adoption of control systems are presented. The subsequent steps include incorporating compressor and turbine off-design curves, along with the aforementioned control systems, to create a more accurate model that closely mirrors real operating conditions..

Chapter 6

Conclusions

In this Master's thesis, various technologies in the field of thermal energy storage have been explored, encompassing both existing and emerging technologies. A novel concept of energy storage has been introduced, wherein excess electricity is stored as sensible heat in a high-temperature man-made tank. This storage system is referred to as the Integrated Thermal Electricity Storage System (IT-ESS), and one of its key features is the ability to utilize components derived from thermoelectric units based on gas turbine technology.

Unlike Pumped Hydro Storage (PHS), which is the most prevalent large-scale energy storage technology, and Compressed Air Energy Storage (CAES), the primary competitor of PHS, IT-ESS does not face geographical constraints and does not rely on fossil fuel inputs. Furthermore, compared to batteries, it is not subject to issues such as low cycle life and self-discharge. However, it is important to note that Flow Batteries may emerge as a viable method of storing large quantities of energy in the near future.

After reviewing the whole spectrum of energy storage technologies and conducting a more thorough analysis of the IT-ESS technology, Chapter 4 introduced various models proposed over the years to describe the behaviour of the storage tank. Subsequently, focusing attention on the model by Benato et al. [24], the modelling of the storage device in Aspen Custom Modeler has been explained. This step is strictly necessary due to the lack of a component able to describe its behaviour in Aspen Plus. After writing the tank model in ACM, it has been integrated with the other components of an IT-ESS within Aspen Plus Dynamics flow-sheet. Then, a few simulations have been performed to simulate charging and discharging processes. The most important results include the temperature distribution inside the tank at different moments of the operation, the absorbed power by the heater and the net power produced in the discharging phase, also function of the turbine inlet temperature. Then, a few sensitivity analyses of flow rate, pressure ratio and tank discretization layers have been presented to evaluate how a change in fixed variables may affect the behaviour of the overall

system, highlighting that the adopted values in the foregoing simulations are not far from the optimal conditions (pressure ratio) or represent a good trade-off between computational time and accuracy (number of layers of the tank). Finally, only a suggestion for future works has been reported for the adoption of control systems.

At the end of the work, the validity of the Integrated Thermal Energy Storage System is tangible, as well as its central role in the energy transitions that we are going to face in the very next years; it will find room in both the industrial and the residential sectors and its range of applicability can be enlarged to stand-alone grids in remote areas, not only in the industrial field. For these reasons, as many aspects as possible of this technology need to be investigated, in order to understand all its potentialities.

In future works, as mentioned in Chapter 5, a more detailed and realistic description of the model will be undertaken. This will involve incorporating heat exchangers in both the charging and discharging phases to provide a more comprehensive estimation of the system's performance. Additionally, the implementation of compressor efficiency maps and Stodola's equation will be carried out to achieve a more accurate depiction of the dynamic behaviour of the plant's components. Lastly, the integration of control systems is strongly recommended, given that this storage system will be integrated into a real electric grid, and thus it must be capable of storing energy from highly variable renewable sources and dispatching it as needed based on the load.

Moreover, other important aspects that need to be studied include the utilization of various materials for the packed bed of the storage device, in order to comprehend the role of the storage material in the system's behaviour, as well as a thermofluid dynamic analysis and experimental tests. Also, further investigation can be carried out on the tank; in particular, regarding a system in which a modular solution for the storage device is adopted: in other words, once the tank overall volume is individuated, it is possible to consider different vessels characterized by a lower volume; in these cases, it is possible to decide which vessels are working in the same moment, an interesting solution in those situations in which the volumes required in different moment of the year are very different from each other; in particular, for the months with a greater production, more vessels can be charged simultaneously, whereas in the months with a lower production, just one or few vessels are used to store the energy.

To conclude, this technology is very promising, but it is still under study. Potential developments in the coming years could significantly contribute to the potential spread of this storage system. Together with existing storage technologies, it will aid the electric grid in accommodating the proliferation of renewable energy power systems, thereby reducing reliance on fossil fuel-powered plants and accelerating the energy transition.

List of Figures

List of Tables

Bibliography

[1] Bo Zhao, Caisheng Wang, Xuesong Zhang, Grid-Integrated and Standalone Photovoltaic, 2018. Distributed Generation Systems.

[2] TERNA, Dati Statistici, (2017) Available on-line at http://www.terna.it/it-it/ sistemaelettrico/statisticheeprevisioni/datistatistici.aspx (accessed September 2017). R. Doherty, M. O'malley, A new approach to quantify reserve demand in systems with significant installed wind capacity, IEEE Transactions on Power Systems 20.

[3] (2005) 587–595, http://dx.doi.org/10.1109/TPWRS.2005.846206.

[4] International Energy Agency. Technology roadmap: Energy storage. 2014. Available online on:www.iea.org (Accessed on October 2017).

[5] International Energy Agency. World energy outlook 2016. 2016. Available online on:www.iea.org (Accessed on October 2017).

[6] Alberto Benato and Anna Stoppato. "Pumped thermal electricity storage: a technology overview". In: Thermal Science and Engineering Progress 6 (2018), pp. 301–315.

[7] Abraham Alem Kebede et al. "A comprehensive review of stationary energy storage devices for large scale renewable energy sources grid integration". In: Renewable and Sustainable Energy Reviews 159 (2022), p. 112213.

[8] Energy storage technologies: An integrated survey of developments, global economical/environmental effects, optimal scheduling model, and sustainable adaption policies Mohammad Amir , Radhika G. Deshmukh , Haris M. Khalid, Zafar Said, Ali Raza, S.M. Muyeen, Abdul-Sattar Nizami Rajvikram Madurai Elavarasan, R. Saidur, Kamaruzzaman Sopian, 2023.

[9] F. Rafik, H. Gualous, R. Gallay, A. Crausaz, A. Berthon, Frequency, thermal and voltage supercapacitor characterization and modeling, J. Power Sources 165 (2) (Mar. 2007) 928–934.

[10] World's largest utility-scale battery energy storage system, Online: https://www. advancedbatteriesresearch.com/articles/22776/worlds-largest-utility-scale -battery-energy-storage-system-now-online.

[11] İbrahim Dinçer and Marc A. RosenThermal, Energy Storage Systems and Applications.

[12] Energy Australia. The principle of pumped hydro storage. URL:http:// theconversation.com/snowy-hydro-gets-a-boost-but-seawater-hydro-could-helpsouth-australia-74442.

[13] Argonne National Laboratory, Compressed air energy storage (caes) in salt caverns, 2009.

[14] Tristan Desrues et al. "A thermal energy storage process for large scale electric applications". In: Applied Thermal Engineering 30.5 (2010), pp. 425–432.

[15] A. Benato, A. Stoppato, Energy and cost analysis of a new packed bed pumped thermal electricity storage unit, Journal of Energy Resources Technology 140 (2) (2018) 020904.

[16] Mehmet Mercangöz et al. "Electrothermal energy storage with transcritical CO2 cycles". In: Energy 45.1 (2012), pp. 407–415.

[17] Matteo Morandin et al. "Conceptual design of a thermo-electrical energy storage system based on heat integration of thermodynamic cycles–Part A: Methodology and base case". In: Energy 45.1 (2012), pp. 375–385.

[18] Wolf-Dieter Steinmann. "The CHEST (Compressed Heat Energy STorage) concept for facility scale thermo mechanical energy storage". In: Energy 69 (2014), pp. 543–552.

[19] Alberto Benato and Anna Stoppato. "Energy and cost analysis of an Air Cycle used as prime mover of a Thermal Electricity Storage". In: Journal of Energy Storage 17 (2018), pp. 29–46.

[20] Singh H, Saini RP, Saini JS. A review on packed bed solar energy storage systems. Renewable Sustainable Energy Rev. 2010;14(3):1059–69.

[21] Desrues T, Ruer J, Marty P, Fourmigué JF. A thermal energy storage process for large scale electric applications. Appl. Thermal Eng. 2010;30(5):425–32.

[22] Benato A. Performance and cost evaluation of an innovative pumped thermal electricity storage power system. Energy 2017;138:419–36.

[23] Sabia G., Heinze C, Alobaid F, "ASPEN dynamics simulation for combined cycle power plant – Validation with hot start-up measurement".

[24] Alberto Benato et al. “TES-PD: A Fast and Reliable Numerical Model to Predict the Performance of Thermal Reservoir for Electricity Energy Storage Units”. In: Fluids 6.7 (2021), p. 256.

[25] J.R. Howell, R.B. Bannerot and G.C. Vliet, Solar-thermal Energy Systems: Analysis and Design. McGraw-Hill, 1982.

[26] Singh, R.; Saini, R.P.; Saini, J.S. Nusselt number and friction factor correlations for packed bed solar energy storage system having large sized elements of different shapes. Sol. Energy 2006, 80, 760–771.

[27] McTigue, J.D.; White, A.J.; Markides, C.N. Parametric studies and optimisation of pumped thermal electricity storage. Appl. Energy 2015, 137, 800–811.

[28] To EW Schumann, “Heat transfer: a liquid flowing through a porous prism”. In: Journal of the Franklin Institute 208.3 (1929), pp. 405–416.

[29] Alexander White, Joshua McTigue and Christos Markides, “Wave propagation and thermodynamic losses in packed-bed thermal reservoirs for energy storage”. In: Applied Energy 130 (2014), pp. 648–657.

[30] Desrues T., Stockage Massif d’électricité sous forme thermique. Ph.D. Thesis, Univeristé de Grenoble, Grenoble, France 2011.

[31] Peccolo S., "Design and management of an Integrated Thermal Energy Storage System", Master’s degree thesis, University of Padua.